Journal of Sound and Vibration 568 (2024) 117895

Contents lists available at ScienceDirect

Journal of Sound and Vibration

journal homepage: www.elsevier.com/locate/jsvi

Aeroacoustics research in Europe: The CEAS-ASC report on 2022 highlights

Christophe Schram [a], Gareth J. Bennett [b,*]

[a] Environmental and Applied Fluid Dynamics, von Karman Institute for Fluid Dynamics, 72 chausséee de Waterloo, Rhode-St-Genèse, 1640, Belgium

[b] Department of Mechanical, Manufacturing and Biomedical Engineering, School of Engineering, Trinity College Dublin, the University of Dublin, Dublin, DO2 PN40, Ireland

ARTICLE INFO

Keywords:
Aeroacoustics
Highlights
CEAS-ASC
Europe

ABSTRACT

The Council of European Aerospace Societies (CEAS) Aeroacoustics Specialists Committee (ASC) supports and promotes the interests of the scientific and industrial aeroacoustics community on a European scale and European aeronautics activities internationally. In this context, "aeroacoustics" encompasses all aerospace acoustics and related areas. Each year the committee highlights some of the research and development projects in Europe.

This paper is a report on highlights of aeroacoustics research in Europe in 2022, compiled from information provided to the ASC of the CEAS. In addition, during 2022, a number of research programmes involving aeroacoustics were funded by the European Commission. Some of the highlights from these programmes are also summarized in this article, as well as highlights from other programmes funded by national programmes or by industry.

Enquiries concerning all contributions should be addressed to the authors who are given at the end of each subsection.

1. Airframe noise

1.1. Trailing-edge noise reduction by locally-applied shallow surface dimples

Airframe noise reduction has driven much research into, e.g., passive noise reduction methods. However, besides the possible noise reduction, many of the proposed methods suffer from an undesirable degradation of the aerodynamic performance. Recently, several publications reported on the drag reduction potential of shallow dimples applied to a flat plate (see Refs. [1,2]). In this contribution, we report on the outcomes of a combined aerodynamic and aeroacoustic investigation [3] carried out on a NACA0012 wing with shallow dimples applied to its aft part (see Fig. 1(a)). Overset-LES [4] was carried out for a chord based Reynolds number Re_c of 4.2×10^5 at zero angle of attack.

The local skin friction coefficient is presented in Fig. 1(b) for both the reference case and the configuration with shallow dimples. Near the dimples, the expected convergent-divergent pattern in the C_f is visible, i.e., decreased (or increased) levels due to decelerating (or accelerating) flow. Amiet's theory of trailing-edge noise suggests that the product of the PSD ϕ_{pp} and coherence length l_z partly quantifies the sound source. This product is presented in Fig. 2(a).

Dimples lead to reduced broadband levels of this product in low-to-mid frequency range. Moreover, the tonal component at approximatively 4.5 kHz is absent for the dimple configuration (due to a coherence breakdown). The far-field directivity revealed

* Corresponding author.
E-mail addresses: christophe.schram@vki.ac.be (C. Schram), gareth.bennett@tcd.ie (G.J. Bennett).

https://doi.org/10.1016/j.jsv.2023.117895
Received 2 June 2023; Accepted 23 June 2023
Available online 1 July 2023

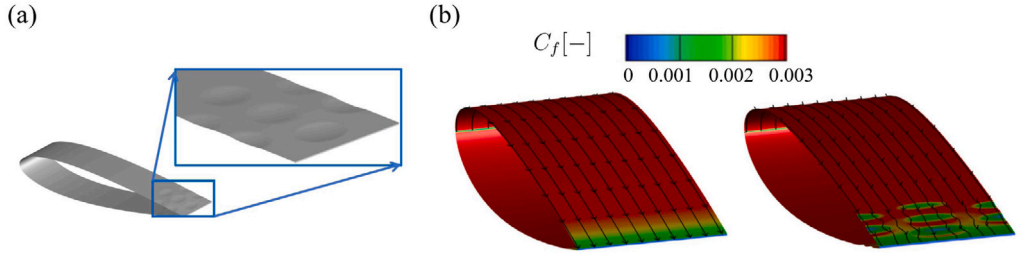

Fig. 1. (a) Shallow dimples applied to the rear part of the NACA0012 wing on both the suction and pressure sides. Inset displays a zoom-in of the dimples. (b) Contour plot of the local skin friction coefficient on the pressure side for the reference and dimple configurations.

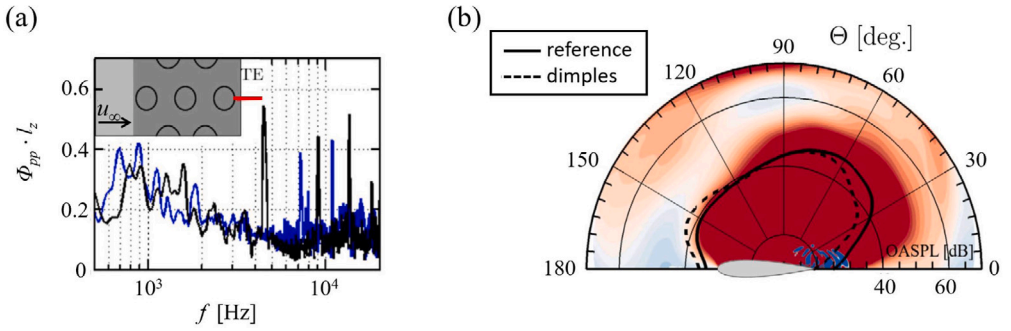

Fig. 2. (a) Comparison of the product $[\phi_{pp} \cdot l_z]$ between reference (black line) and dimple (blue line) configurations at a constant stream-wise location ($x/c = 0.99$). The inset shows the span-wise location where the PSD was extracted. (b) OASPL directivity plot with contours representing the instantaneous pressure fluctuations. The OASPL is based on a frequency range between 500 Hz and 10 kHz and presented for an observer at 1 m distance. (For interpretation of the references to colour in this figure legend, the reader is referred to the web version of this article.)

that the dimple treatment results in an OASPL reduction of approx. 5.5 dB in the downstream direction and a 3.5 dB increase in the upstream direction. These effects have a favourable impact on the trailing edge noise reduction, however, at the cost of 2 drag counts. To conclude, this contribution argues for the inclusion of shallow dimples to the list of viable passive noise reduction methods (e.g., porous materials and finlets).

Written by R. A. D. Akkermans: rinie.akkermans@haw-hamburg.de, Hamburg University of Applied Sciences, Germany, and V.B. Ananthan, DLR, Germany.

1.2. Noise of load-adaptive wind turbine blade sections

In the project *SmartBlades 2.0*, the noise of load-adaptive blade sections was investigated in response to the demand of wind turbines with large diameter rotor. Two load-adaptive technologies were studied: a plain flap at the outer radius of the blade, a dominant wind turbine rotor noise source [5], and a slat at the inboard rotor, which delays flow separation and improves aerodynamic efficiency [6].

A small-scale blade section (1200 mm span, 300 mm chord) was tested in the Acoustic Wind Tunnel Braunschweig (AWB) to investigate the acoustic effect of a midspan deployed flap (400 mm span, 90 mm chord), Fig. 3(a). Dedicated noise reduction technologies, a replaceable porous flap side-edge (FSE) and trailing-edge (TE) brushes were used to allow a sufficient distinction between selected noise sources in the experiment. In the laboratory condition, the FSE noise is insignificant for the flap deflection angles of ±5° to contribute to the far-field noise [7]. The numerical method, FRPM/FMCAS (Fast Random Particle Mesh/Fast Multipole Code for Acoustic Shielding) [9], was proven successful to predict the measured TE noise and, in isolation, the FSE noise, Fig. 4 [8].

In the second application FRPM/FMCAS was used for a comparative study between inboard slat noise vs. outboard TE noise of a full-scale rotor under operational conditions, Fig. 3(b) [8]. Using the acoustic simulation of stationary rotor sections of 1 m span, their respective acoustic footprints were calculated for one revolution of the rotor applying a simple and fast inhouse wind turbine noise prediction method [10]. According to Fig. 5 the slat noise adds 1 dBA at wind speed $U_0 = 9$ m/s wind speed and is negligible for lower speeds. At an off-design configuration with $U_0 = 16$ m/s, the slat noise contributes more than the outboard TE noise.

Written by A. Suryadi: alexandre.suryadi@dlr.de, M. Herr, DLR, Germany.

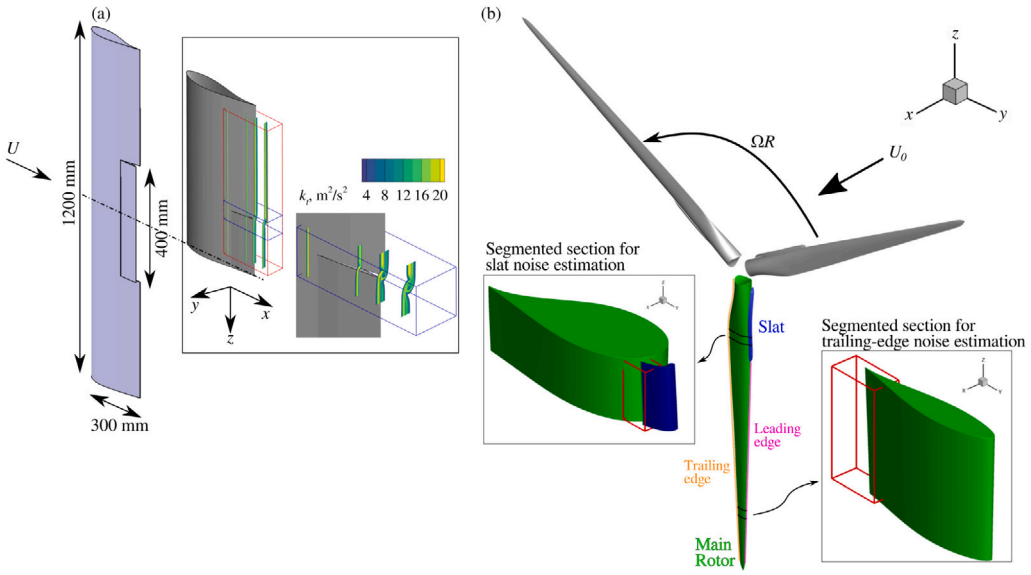

Fig. 3. (a) Schematic of the blade section model with midspan flap studied in Refs. [7,8], and (b) the simulated rotor in operational condition in Ref. [8]. The domains for noise estimation are framed. k_t: Turbulent kinetic energy, U: wind tunnel velocity, ΩR: angular velocity, and U_0: wind speed.

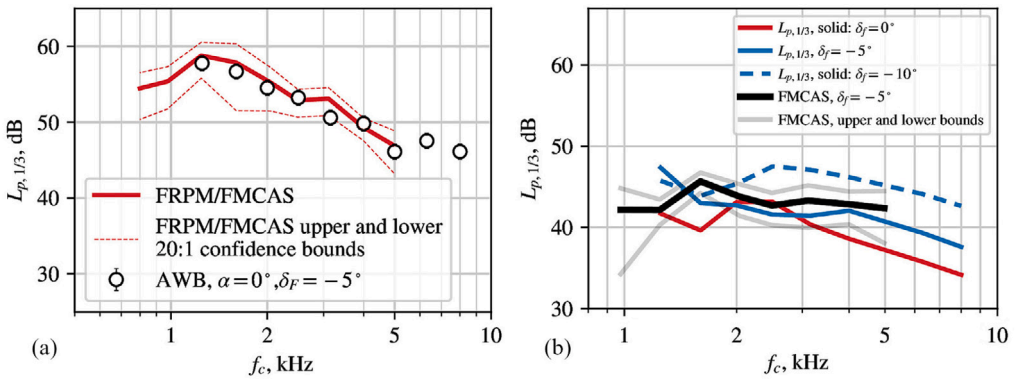

Fig. 4. Comparison between measurement and simulation of (a) third-octave band sound pressure levels $L_{p,1/3}$ of the main element and −5° deflected flap, (b) $L_{p,1/3}$ of an isolated flap side-edge noise. Upper and lower bounds indicate 20:1 confidence levels.

1.3. Cylinder vortex shedding noise reduction by unstructured porous coatings

The tonal noise generated due to periodic vortex shedding from circular cylinders in a flow is a major aeroacoustic problem. It occurs, for example, at the aircraft landing gear or at the pantograph of high-speed trains. One method to reduce this noise is the use of porous coatings. In a number of wind tunnel studies, the noise generated by circular cylinders coated with open-porous materials of different permeability and porosity [11–13] as well as their effect on the surrounding flow field was investigated. Porous coated cylinders with high permeability and porosity significantly reduce both broadband and tonal noise. The vortex shedding peak is observed to shift and narrow (see Fig. 6), the latter being due to an increase in spanwise coherence.

In a recent numerical simulation [14], the additional influence of the thickness of the porous coatings was investigated by means of detailed Large Eddy Simulations. It was found that, in general, an optimum selection of coating thickness and permeability can lead to a notable noise reduction, although the choice of the porous material in terms of its permeability is more important than the selection of the porous layer thickness, as materials with extremely low permeability will not lead to noise reduction at all. Furthermore, the simulations enabled the analysis of the flow inside the porous media and thus a better understanding of the physical mechanisms. It was observed that porous materials with high permeability stabilize the vortex shedding (see Fig. 7) and show vortices being shed from the inner core cylinder. In addition to the use of unstructured porous coatings, investigations on

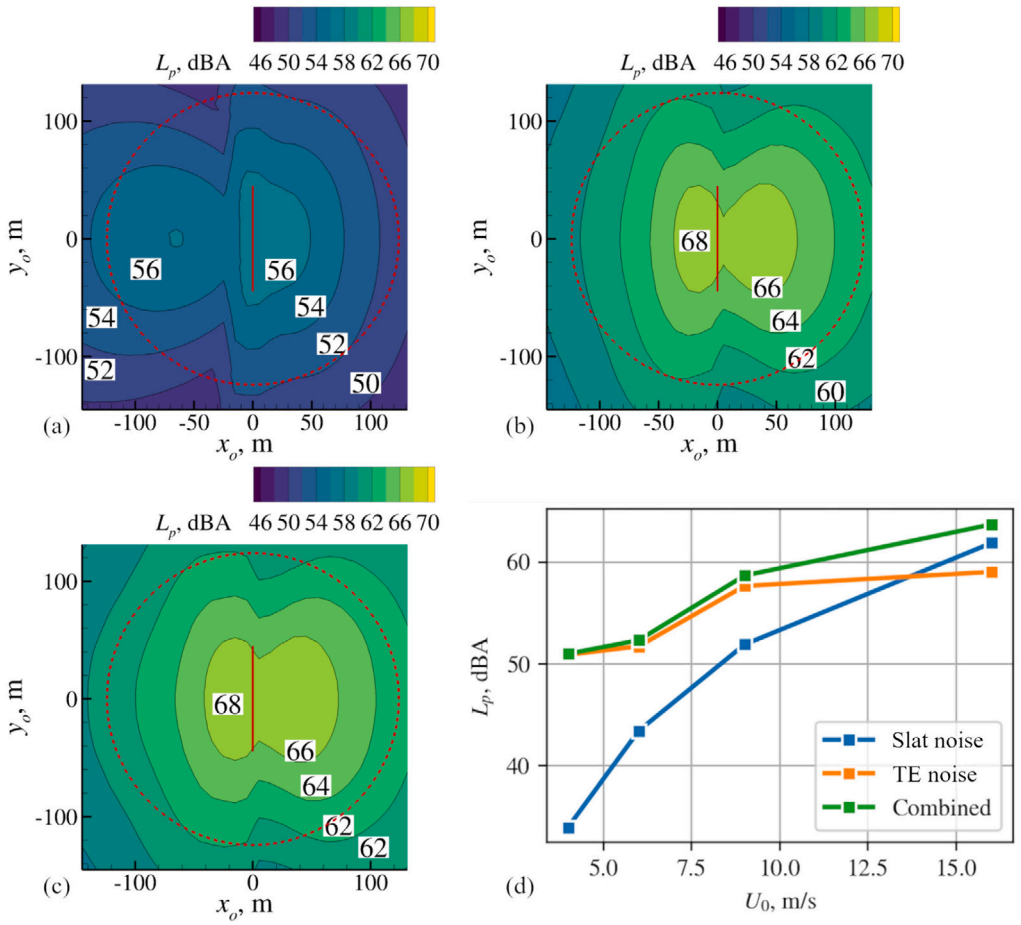

Fig. 5. The overall sound pressure level L_p footprint from (a) only the slat noise, (b) only the outboard trailing-edge noise, (c) both noise sources, for wind speed of 9 m/s, and (d) the overall sound pressure level at $x_o = 124$ m and $y_o = 0$ m for all wind speed cases. The wind direction in (a)–(c) is from left to right.

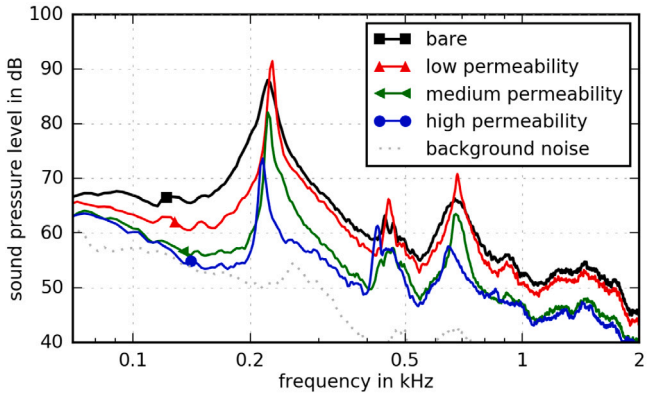

Fig. 6. Sound pressure level spectra obtained at a Reynolds number (based on outer cylinder diameter) of 1.27×10^5, measured with a single microphone at a distance of 0.61 m at 90 degrees to the flow.

the use of structured porous coatings have begun [15,16]. Such additively manufactured coatings have similar properties as the unstructured materials, but allow for a better visualization of the flow inside the medium.

Written by Thomas F. Geyer, (thomas.geyer@dlr.de), DLR, Germany, Sparsh Sharma, University of Cambridge, UK, Elias J. G. Arcondoulis, University of Bristol, UK.

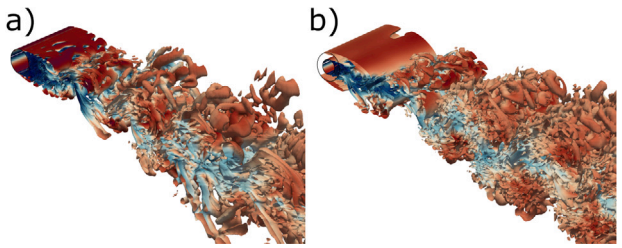

Fig. 7. Iso-surfaces of the vortex structures based on the Q-criterion at $Q = 0.5$ (coloured by the instantaneous velocity contour at the end of the simulated time) for (a) bare reference cylinder and (b) cylinder with highly permeable porous coating.

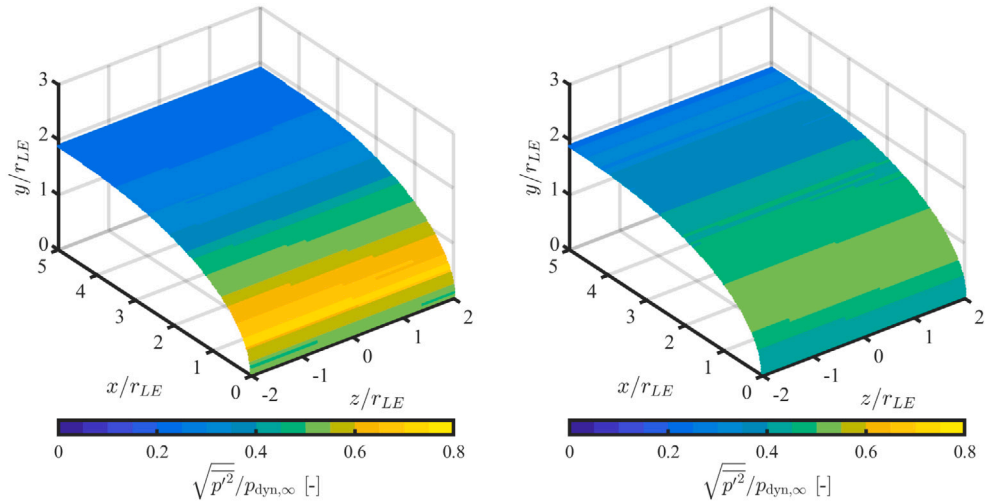

Fig. 8. R.m.s. pressure-fluctuations contours on the surface of a solid (on the left) and porous (on the right) airfoils made dimensionless by the free-stream dynamic pressure.

1.4. Effect of porosity on Curle's dipolar sources on an airfoil in turbulent flow

The aerodynamic noise radiated by an airfoil interacting with inflow turbulence can be mitigated by integrating flow-permeable materials into its structure [17–19]. When a compact porous body is accounted for in Curle's acoustic analogy to predict this source of noise, a dipole corresponding to the non-zero unsteady Reynolds stresses appears on the surface [20,21]. This equivalent source acts concurrently with the dipole associated with the pressure fluctuations. However, its relative contribution to the far-field noise remains unclear.

This research has the objective to, on the one hand, investigate the impact of porosity on the unsteady surface pressures of a thick airfoil interacting with upstream turbulence and, on the other hand, evaluate the efficiency of the Reynolds-stresses surface term as a sound-production mechanism. Large-eddy simulations of a rod-airfoil configuration revealed that the peak of surface-pressure fluctuations is effectively mitigated by the porous treatment (see Fig. 8). This attenuation is mostly confined to the low-frequency range of the spectrum and is caused by the weaker distortion of the incoming eddies [22]. Nevertheless, the porous treatment only marginally affects the spanwise coherence or in-phase behaviour of the unsteady pressures at the vortex-shedding frequency of the upstream cylinder.

The Reynolds-stresses term on the surface is found to be non-negligible in the stagnation region, where the transpiration velocity is higher. Interestingly, although its amplitude is considerably smaller than that of the pressure-fluctuations term, the two sources exhibit partial correlation in the front part of the wing profile (see Fig. 9), suggesting the presence of constructive interference that contributes to the far-field noise radiated by the porous airfoil for observation angles near the stagnation streamline.

The conclusions drawn in this research eventually offer valuable insight into the design of novel and more effective passive strategies to reduce turbulence-interaction noise and can be relevant to industrial applications.

Written by Riccardo Zamponi, (riccardo.zamponi@vki.ac.be), VKI, Belgium.

1.5. Airfoil tip vortex noise reduction using end plates

When a three-dimensional airfoil with a free end is subject to a flow at moderate to high angles of attack, fluid starts to flow from the region of high pressure on the pressure side towards lower pressure at the suction side around the airfoil tip, leading to

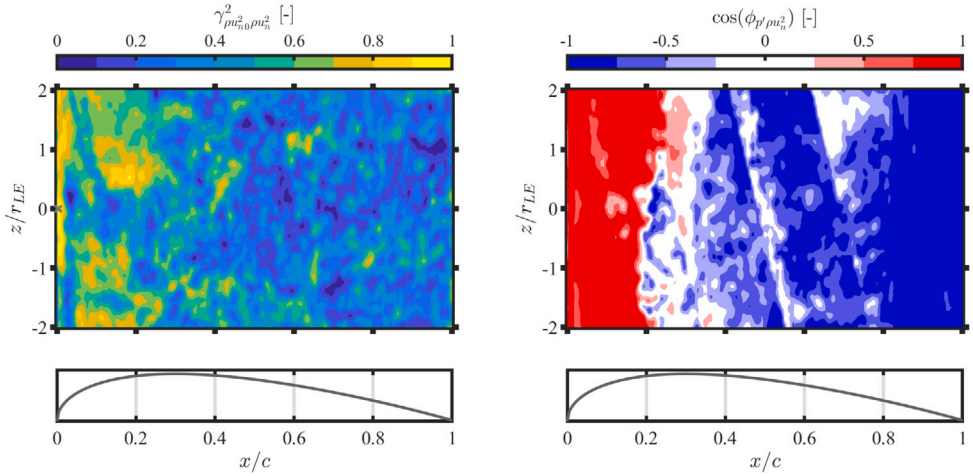

Fig. 9. Coherence (on the left) and phase-difference (on the right, expressed with the cosine function) contours between the unsteady-pressure and Reynolds-stresses terms on the surface of the porous airfoil at $St = 0.2$.

the formation of a so-called tip vortex. The subsequent interaction of this tip vortex with the trailing edge of the airfoil leads to strong tonal noise, characterized by a broad hump in the far-field acoustic spectra at high frequencies [23]. This is an important noise source mechanism especially for aircraft high lift devices such as flaps and for rotating machinery such as fans or rotors. In a number of detailed wind tunnel studies [24,25], the effect of side plates on the reduction of tip vortex trailing edge noise from symmetric and cambered wall-mounted finite airfoils was examined at subsonic flow speeds using microphone array measurement techniq ues, constant temperature anemometry measurements in the wake as well as surface flow visualizations. It was found that the end plates greatly reduce the transfer of fluid from the pressure side to the suction side and, subsequently, diffuse the vorticity and reduce the influence of flow structures forming at the free end of the airfoil. Thus, the resulting flow field resembles that of a two-dimensional configuration (see Fig. 10). Although the exact shape of the end plate did not have a strong effect on the tip noise reduction efficiency, the results showed that configurations for which the end plates are pointed towards the suction side are more efficient (see Fig. 11), as configurations with pressure side end plates still lead to a noise contribution at higher angles of attack.

Written by Erik W. Schneehagen (erik.w.schneehagen@tu-berlin.de), Technische Universität Berlin, Germany, Thomas F. Geyer, DLR, Germany, Ennes Sarradj, Technische Universität Berlin, Germany.

2. Propeller noise

2.1. Multi-fidelity methods for the aeroacoustics of transitional rotors

Researches in the field rotor aeroacoustics in transitional flow regime were conducted to isolate the effects related to the occurrence of a laminar separation bubble on the rotor blades, and improve the associated broadband noise prediction. Following the definition of a benchmark configuration and a preliminary evidence of a broadband noise contribution due to the presence of a laminar separation bubble [26], additional experimental investigations were carried out to confirm the initial intuition [27,28].

In parallel, scale-resolving Lattice-Boltzmann (LB) simulations were conducted using an industrial LBM solver, with the intent to scrutinize the effects related to a non-axial flow condition [29], and the predictive capabilities of the solver in a broad range of operational conditions [30]. The latter analyses revealed some limitation of standard version of the LBM solver, which were finally overcome in a new version of the solver [31]. The last effort led to a very accurate prediction of the far-field noise spectrum over a very broad frequency range, including the broadband noise hump induced by the laminar separation. It is worth mentioning that, the improvement of the high-fidelity prediction capabilities have been facilitated by a deep knowledge of the specific aeroacoustic physics gained through the development of low-fidelity methods [26,32].

Written by Damiano Casalino: D.Casalino@tud.nl, Delft University of Technology, Netherlands.

2.2. Mach number effects and neural network modelling of propellers acoustic emissions

This work presents a numerical investigation of noise radiated by two side-by-side propellers, suitable for Distributed-Electric-Propulsion concepts [33]. The focus is the assessment of the effects of blade tip Mach number on the radiated noise when the direction of rotation, the relative positions between the hubs, and the relative phase angle between the blades of the propellers are changed. The aerodynamic analysis is performed through a potential-flow-based boundary integral formulation, which is able to

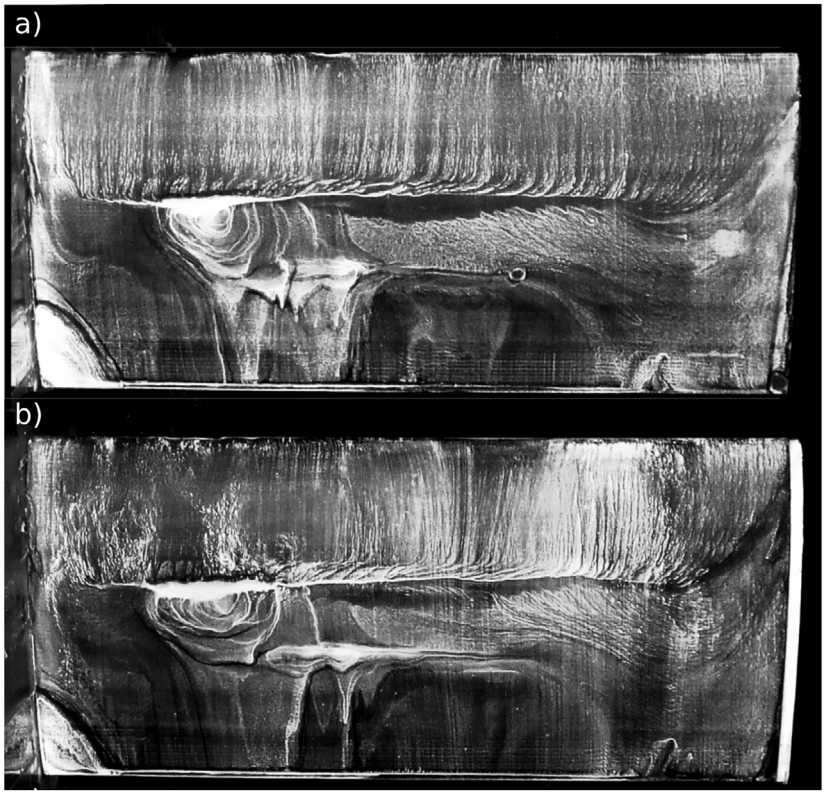

Fig. 10. Surface flow visualization for NACA 4412 airfoil at $Re = 150,000$ and angle of attack 10 degrees, suction side, flow from top to bottom, left side wall, right side free end, (a) baseline configuration, (b) end plate on the pressure side.

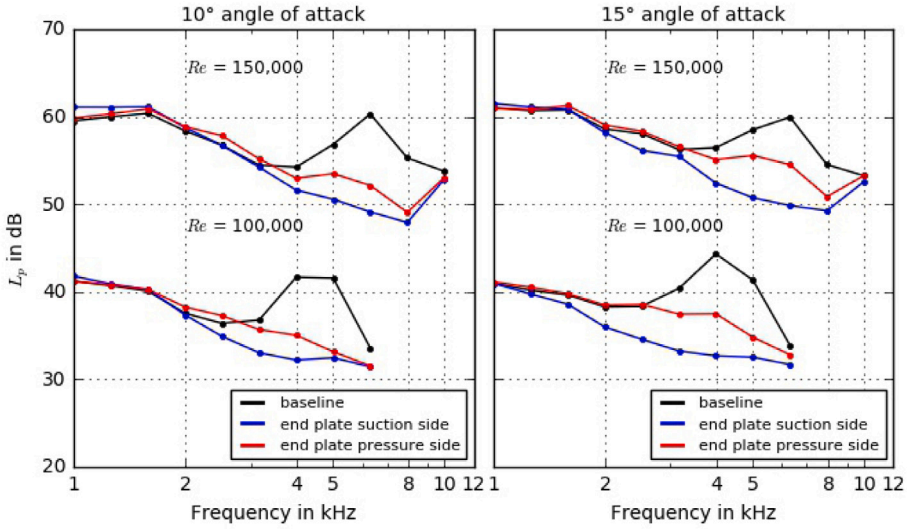

Fig. 11. Third octave sound pressure levels obtained by integration over the whole airfoil (between each flow speed 10 dB are added to avoid overlay).

model severe body-wake interactions [34]. The noise field is evaluated through a boundary-integral formulation for the solution of the Ffowcs Williams and Hawkings equation [35]. The numerical investigation shows that the blade tip Mach number strongly affects the magnitude and directivity of the radiated noise. In addition, the increase of the tip-clearance increases the spatial frequency

Fig. 12. Photograph of overlapping rig inside the ISVR anechoic chamber.

of the noise directivity at the two analysed tip Mach numbers for both co-rotating and counter-rotating configurations. Finally, for counter-rotating propellers, the relative phase angle between the propeller blades provides a decrease of the averaged emitted noise [36], regardless the tip Mach number. One of the main results achieved is the scalability with the blade tip Mach number of the influence on the emitted noise of the considered design parameters.

In the framework of Simulation-Based-Design applied to aircraft, the use of meta-models provides an efficient and accurate alternative to demanding simulations or experiments, making it suitable for optimization applications. In this context, the aim of this research is the development of a general methodology to be adopted since the earlier design phases, which can predict the acoustic emissions of Distributed-Electric-Propulsion systems [37], combining the accuracy of high-fidelity numerical tools with the computational efficiency of surrogate models [38].

Here, the surrogate models are synthesized through Deep Neural Networks using feed-forward and recurrent architectures. The numerical database used for training purposes is obtained by an aerodynamic tool for potential-incompressible flows [34] coupled with the Farassat 1 A boundary integral formulation for the noise field evaluation [39]. The work was focused on the development of surrogate models with different architectures, comparing them in terms of accuracy and computational efficiency, able to capture the effect of propeller geometric parameters and operative conditions changes on the acoustic emissions of a six counter-rotating propellers array configuration.

The numerical investigation demonstrated that the synthesized surrogate models accurately predict the noise emissions of the multi-propeller configuration with reduced computational costs. It also shows that the fully-connected feed-forward network is the best approach to synthesizing metamodels suited for noise emissions prediction, providing more accurate results regardless of the algorithm adopted for the network optimization. On the other hand, the recursive network accurately predicts the primary trend of the directivity but does not the wavy behaviour.

Written by Caterina Poggi: caterina.poggi@uniroma3.it, M. Gennaretti and G. Bernardini, Università Roma Tre, Italy.

2.3. On the optimum separation distance for minimum noise of contra-rotating rotors

Overlapping rotor systems are currently used on some urban flight vehicles and will become increasingly common in future electric propulsion, since they provide one of the most compact platform volumes per thrust. The noise radiation mechanisms due to two closely coupled rotors are complex owing to the potentially large number of distinct self-noise and interacting sources (see Fig. 12).

Motivation for this work comes from a previous experimental preliminary study [40] that investigated the influence of axial and radial separation distance on the radiated noise of two overlapping propellers. The balance of sources for low-noise in a co-axial configuration is investigated in this work [41]. The simple scaling law, $N^{5.5}D^{7}$, has also been found to describe the measured variation in total radiated sound power versus the rotor RPM N and the rotor diameter D (see Fig. 13).

Based on measurements of the overall sound power level for a range of rotor thrusts and diameters, this work has identified separation distances approximately in the range $0.25 < z/D < 0.5$ where the noise radiated is a minimum and the aerodynamic efficiency is high. This range of separation distances is attributed to an optimum balance between the various dominant sources. A source breakdown is performed and shown in Fig. 14, which a compares the overall sound power levels plotted against z/D at a fixed thrust setting of 16 N for the two rotors operating simultaneously and at respective thrust individually.

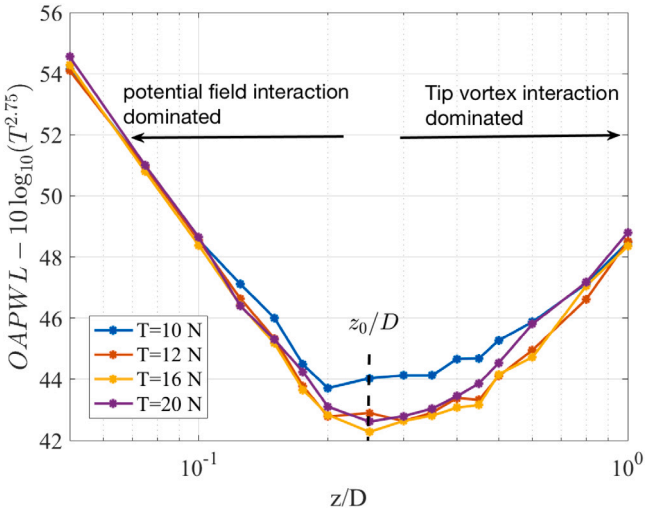

Fig. 13. Overall sound power level variation with separation distance at various combine total thrust for 16-in diameter rotor.

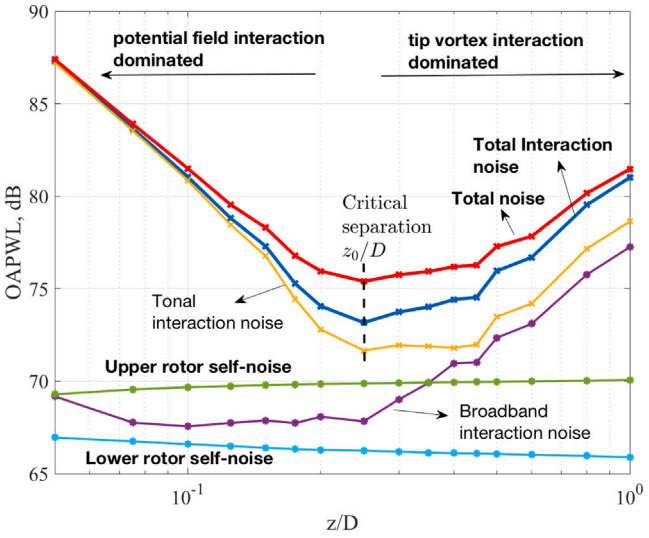

Fig. 14. Overall sound power level variation for various sources with separation distance at a fixed combined thrust of 16 N.

The potential field interactions are shown to dominate overall noise at separation distances smaller than the optimum distance, $z/D < z_0/D$, while the noise due to tip vortex interaction is dominant for distances greater than the optimum value, $z/D > z_0/D$. A simple semi-empirical framework has been proposed to validate this hypothesis as shown in Fig. 15. Very good agreement is observed in the general trends, demonstrating that at the optimum separation distance of $z/D \approx 0.25$ all interaction noise sources contribute almost equally to the overall noise.

Written by P. Chaitanya: c.c.paruchuri@soton.ac.uk, P. Joseph, S.D. Prior, A.B. Parry, ISVR, University of Southampton, United Kingdom.

3. Fan and jet noise

3.1. Downstream porosity for the reduction of turbulence–airfoil interaction noise

Broadband turbulence interaction noise is one of the dominant noise sources in several aerospace applications such as modern turbofan engines. Leading edge serrations and porosity have proved to be effective technologies for reducing broadband interaction noise. These however often involve an aerodynamic penalty since most of the lift is generated in the leading edge region. This motivated the idea of introducing a porous section downstream of the leading edge, thereby reducing adverse effects on aerodynamic performance. This was first proposed in [42] and later extended in [43] and a companion analytical study [44]. Recent experimental

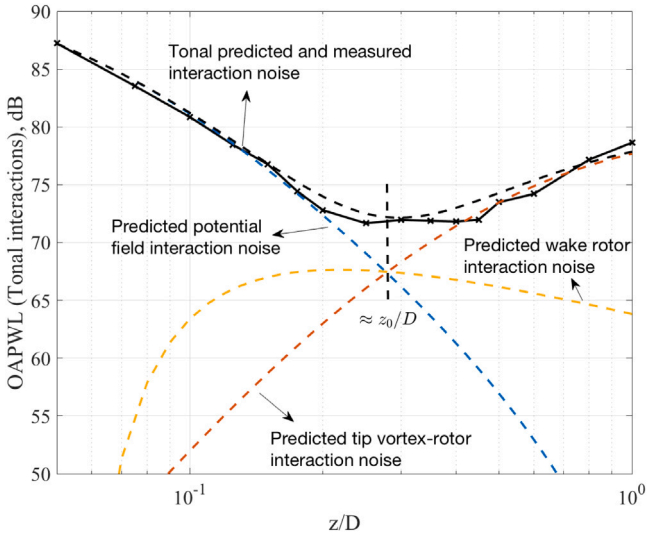

Fig. 15. Comparison between measured and predicted overall sound power levels for tonal interaction noise source with separation distance z/D at combined thrust of 16 N.

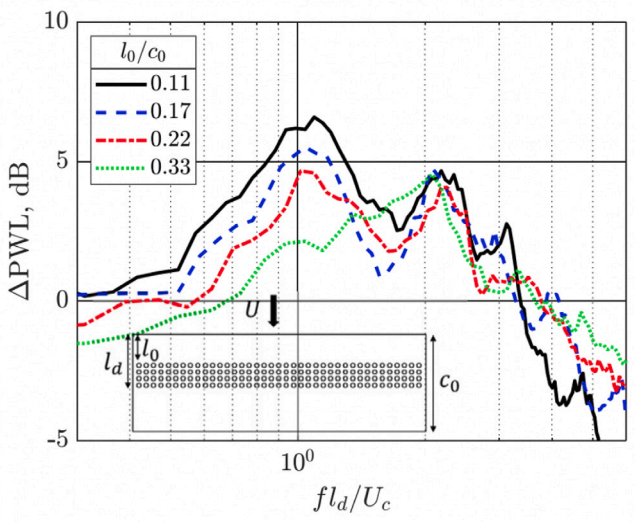

Fig. 16. Sound power noise reduction spectra for $l/c_0 = 0.12$, 40 m/s and various values of l_0 for porous flat plates with D = 3 mm and T/D = 2.5 mm.

work on flat plate and thin airfoils with downstream porosity [45] found that the noise reduction spectra collapse when plotted against non-dimensional frequency fl_d/U_c (Fig. 16), where l_d is the distance between the leading edge and the downstream edge and U_c is the convection velocity.

Narrowband peaks of noise reduction were identified at $fl_d/U_c \approx n$, where n is an integer. A new noise reduction mechanism was proposed to explain the additional π phase shift required to explain this result, in which interactions downstream of the leading edge are due to secondary vorticity. These peaks were observed to be superimposed on a broad 'envelope', whose spectral shape was shown to be closely related to the noise reduction due to a shorter chord equal to that of the upstream section of length l_0.

An analytical model was proposed based on interference between two leading edge sources Δp_0 and Δp_{l_d}, cut-off radiation along the porous section and an effective shortening of the chord, as shown in Fig. 17. The model was found to capture the general behaviour of the measured noise reduction spectra (Fig. 18).

Written by S. Palleja-Cabre: s.palleja-cabre@soton.ac.uk, P. Chaitanya, P. Joseph, J.W. Kim, ISVR, University of Southampton, United Kingdom, M.J. Priddin, L.J. Ayton, University of Cambridge, United Kingdom, T.F. Geyer, Brandenburg University of Technology Cottbus, Germany, T.P. Chong, Brunel University London, United Kingdom.

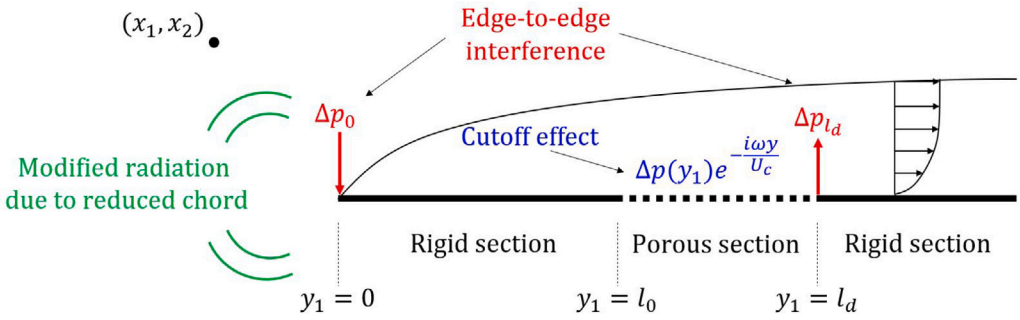

Fig. 17. Summary of source regions and mechanisms of noise reduction.

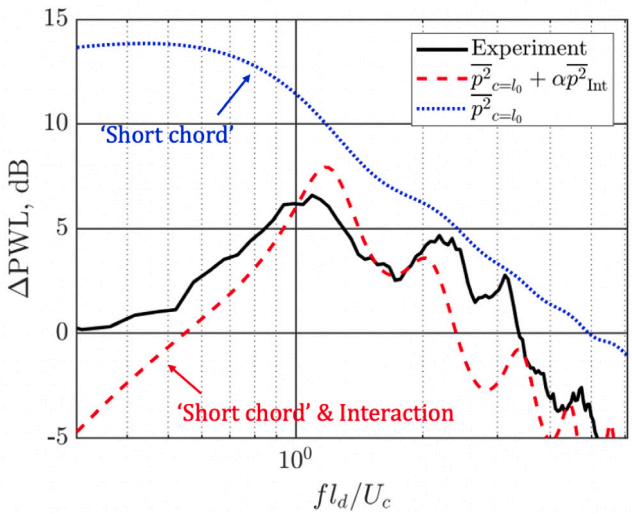

Fig. 18. Comparison of the measured and predicted sound power noise reduction spectra for $l_0/c_0 = 0.11$, $l/c_0 = 0.12$ and 40 m/s for a porous flat plate with D = 3 mm and T/D = 2.5 mm.

4. Liners and metamaterials

4.1. Spatially-varying impedance model for locally reacting acoustic liners at a high sound intensity

The spatial variation of acoustic liner impedance in aeroacoustic ducts at high sound pressure levels (SPLs) has been recently investigated in Ref. [46]. It is shown that impedance discontinuity between a rigid wall and the liner is a leading factor in defining the impedance variation in space. A large impedance discontinuity results in a high variation of the normal acoustic component of the velocity, which induces strong nonlinear effects. An iterative numerical model inspired by previous work [47,48] was proposed to predict the spatial acoustic impedance over a liner and was validated with measurements of acoustic velocity fields obtained using laser Doppler velocimetry (LDV). The model was explored on numerical examples and showed that the impedance discontinuity is a significant driver of nonlinear response, and that the convergence of the iteration process is more difficult to reach for low resistivity liners. The nonlinear impedance effect is less pronounced in ducts with lower height, due to the opposite wall boundary condition cancelling the high variation of normal component of the velocity. The direction of the flow relative to the wave propagation seems to play a role in the space-dependent impedance, due to the intricate relationship between the wave and the normal mean flow velocity gradient. Could this be one of the reasons why there is a mismatch between impedance eduction results observed when the wave direction relative to the flow is changed [49]? The iterative space-dependent impedance model showed an improvement in goodness of fit on the LDV data, when compared to the classical constant impedance model, and provides more meaningful information for the liner designer. The incident SPL is thus not the only factor to predict the acoustic response of a liner, and liner characterizations should aim to decouple the effect of flow, SPL, measurement technique and bench dimensions.

Written by Rémi Roncen: remi.roncen@onera.fr, ONERA/Département Multi-Physique pour l'Énergétique, Université de Toulouse, F-31055, Toulouse, France, and Fabien Méry, Estelle Piot, ONERA/Département Multi-Physique pour l'Énergétique, Université de Toulouse, F-31055, Toulouse, France, and Patricia Klotz, ONERA/Département Traitement de l'Information et Systèmes, Université de Toulouse, F-31055, Toulouse, France.

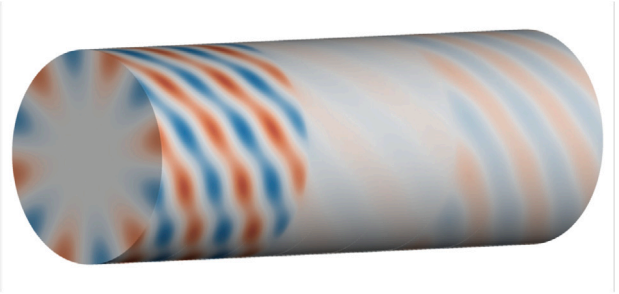

Fig. 19. High-order acoustic mode propagation and attenuation computed by CFD in the CANNELLE flow duct. The central part of the duct is covered with an acoustic liner.

4.2. Acoustic mode attenuation in ducts using CFD with time-domain impedance boundary condition

Covering some parts of the engine nacelle with sound-absorbing materials, called "liners", is one of the most effective solutions for reducing the noise of turbofan engines. It is therefore very important, from a practical point of view, to be able to take into account the effect of a lined surface in the simulations carried out for the design of the engine nacelle. If it is already difficult to do so in single frequency Computational AeroAcoustics(CAA) simulations, it is even more difficult with time-domain Computational Fluid Dynamics (CFD) codes. [50] has opened the way by implementing in a unsteady Reynolds-averaged Navier–Stokes equations (URANS) solver a parametric Time-Domain Impedance Boundary Condition (TDIBC) by generalizing a conventional solid wall boundary condition. In the work highlighted here [51], an alternative approach based on a Navier–Stokes Characteristic Boundary Condition (NSCBC) formalism has been developed. The TDIBC is based on the Oscillo-Diffusive Representation (ODR) of a liner [52], which provides an intrinsically broadband representation of its acoustic response. The ODR-TDIBC is implemented in an industrial URANS finite volume CFD solver, and special care has been taken to time implicitation of the equations, so that the TDIBC formulation does not have a significant impact on numerical stability or computation time. The ability of the solver to correctly predict the attenuation of acoustic modes (see Fig. 19) has been validated using 2D and 3D simulations of flow ducts, showing close alignment with results from a CAA code and with experiments.

Written by Estelle Piot: estelle.piot@onera.fr, ONERA / DMPE, Universite de Toulouse, F-31055 Toulouse , France.

5. Techniques and methods in aeroacoustics

5.1. Gaussian-based machine learning algorithm for the design and characterization of a porous meta-material for acoustic applications

In the context of environmental noise reduction, porous media with embedded periodic inclusions acting as local resonators have gained great attention [53]. This configuration is known as meta-material. Although the wide research nowadays focused on meta-materials, the lack or incompleteness of analytical formulations to estimate acoustic indicators often pushes towards the use of numerical simulations or experimental tests, requiring financial expenses, computational power and time, setup of experimental campaigns, etc. As reported by Bianco et al. [54], this opens the way to the use of alternative techniques, such as machine learning, able to provide automated and quick predictions, fundamental in preliminary design phases or more advanced characterization tasks. This work investigates the applicability of Gaussian processes as tools to perform the characterization in terms of transmission loss peak frequency and percent increase (with respect to the homogeneous configuration) of meta-material acoustic packages in which the porous phase is described with Delany–Bazley–Miki (DBM) and Johnson–Champoux–Allard (JCA) models [55]. The characterization procedure exploits a procedure merging analytical and numerical approaches and machine learning (shown in Fig. 20).

The predictions provided by Gaussian processes are below 5% moreover, the complexity increase, consequence of the switch from DBM to JCA model, allows a noticeable reduction of the number of training examples. The histogram of the errors for the JCA case is reported in Fig. 21. These results prove that machine learning approaches can provide automated and fast estimations of acoustic indicators and that a thorough choice of the features can not only improve the predictions, but also reduce the number of training examples.

Written by A. Casaburo: alessandro.casaburo@ec-lyon.fr, École Centrale de Lyon, France, D. Magliacano, G. Petrone, F. Franco, S. De Rosa, Università degli Studi di Napoli Federico II, Italy .

5.2. Correction for sensor-size-related attenuation of wall pressure spectra measurements

Turbulent boundary layer (TBL) induced wall pressure spectra were measured using sensors of different sizes, types, and mounting configurations, aiming to quantify the spectral attenuation caused by signal averaging over the sensor surface [56]. Based on the reference spectra measured with a pinhole-mounted sensor, the attenuation spectra for different sensors were calculated, and the

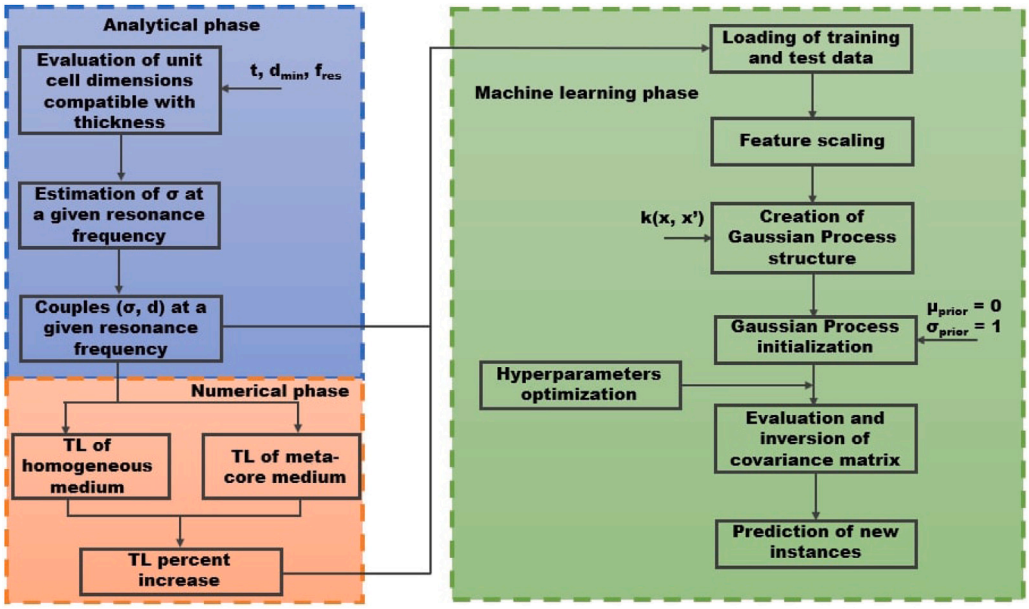

Fig. 20. Flowchart of the characterization procedure.

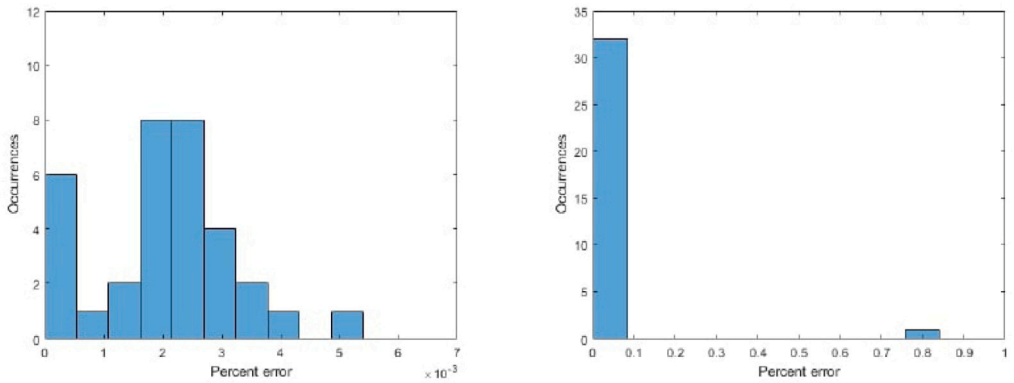

Fig. 21. Predictions errors when predicting the resonance frequency (left) and the transmission loss percent peak increase (right).

results show that the attenuation is larger for sensors with a larger sensing area and for a flow with a lower freestream velocity, see Fig. 22. It was demonstrated that an adverse pressure gradient increases the attenuation significantly, whereas a favourable pressure gradient has no noticeable effect on the attenuation.

According to Corcos [57], the sensor radius r and the convection velocity U_c are the key parameters for calculating the attenuation. In practice, non-uniform sensitivity over the sensor surface (not considered by Corcos) can significantly reduce the effective sensing area. This issue was discussed from the theoretical point of view, and the effective radius of sensors was suggested. Furthermore, the fact that U_c depends strongly on the flow condition (see Fig. 23) is of great importance for determining the attenuation. A convection velocity model was proposed, including Reynolds number and pressure gradient effects. A scaling factor for the sensor-size dependence was suggested to determine U_c applied to different sensors.

Finally, a correction model as a function of TBL-dependent parameters was proposed, which can be applied to a wide range of flow conditions and commonly used sensor types. To assess the present correction model, four test cases were selected which were measured at different facilities with different sensor types, covering a wide range of Reynolds numbers. The results show that spectral attenuation can be corrected with the model by more than 20 dB with high accuracy, see Fig. 24.

Written by Nan Hu: nan.hu@dlr.de, DLR, Germany.

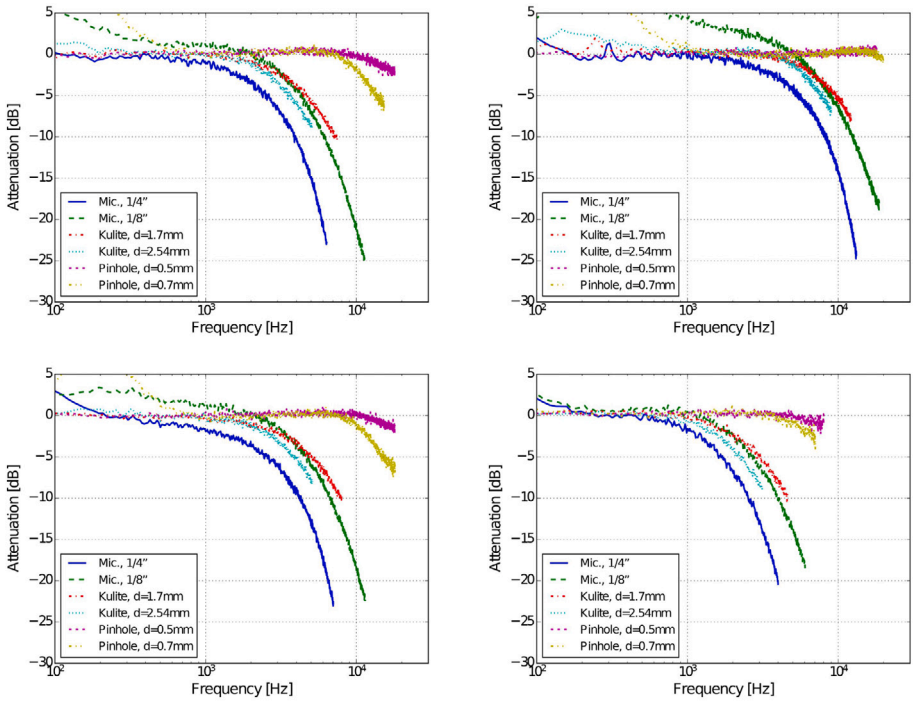

Fig. 22. Attenuation spectra, (top left) zero pressure gradient, $U_0 = 30$ m/s (top right) zero pressure gradient, $U_0 = 60$ m/s (bottom left) favourable pressure gradient, $U_0 = 30$ m/s (bottom right) adverse pressure gradient, $U_0 = 30$ m/s.

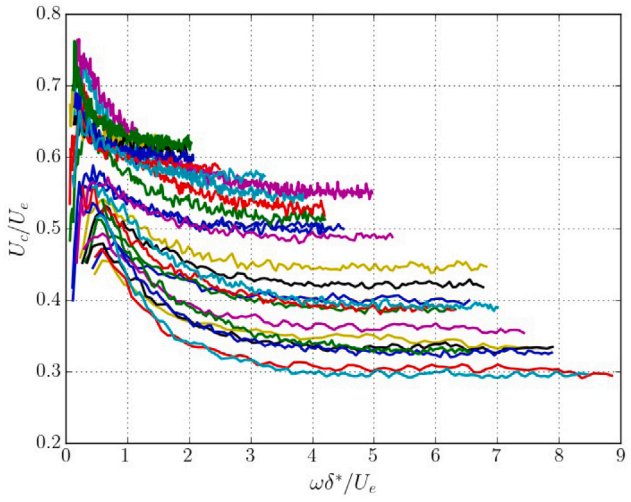

Fig. 23. Convection velocity for flows with zero, favourable and adverse pressure gradients.

5.3. Compensation of modelling errors for the aeroacoustic inverse problem with tools from deep learning

In the field of aeroacoustic source imaging one seeks to reconstruct acoustic source powers from microphone array measurements. For most setups one cannot expect a perfect reconstruction. The main effects that contribute to this reconstruction error are data noise and modelling errors. While the data noise is accounted for in most advanced reconstruction methods e.g. by a proper regularization strategy, the modelling error is usually neglected. This article [58] proposes an approach that extends regularized inverse methods [59] with a mechanism that takes modelling error into account. The presented algorithmic framework utilizes the representation of the FISTA algorithm [60] by a neural network and uses standard gradient schemes from the field of deep learning [61].

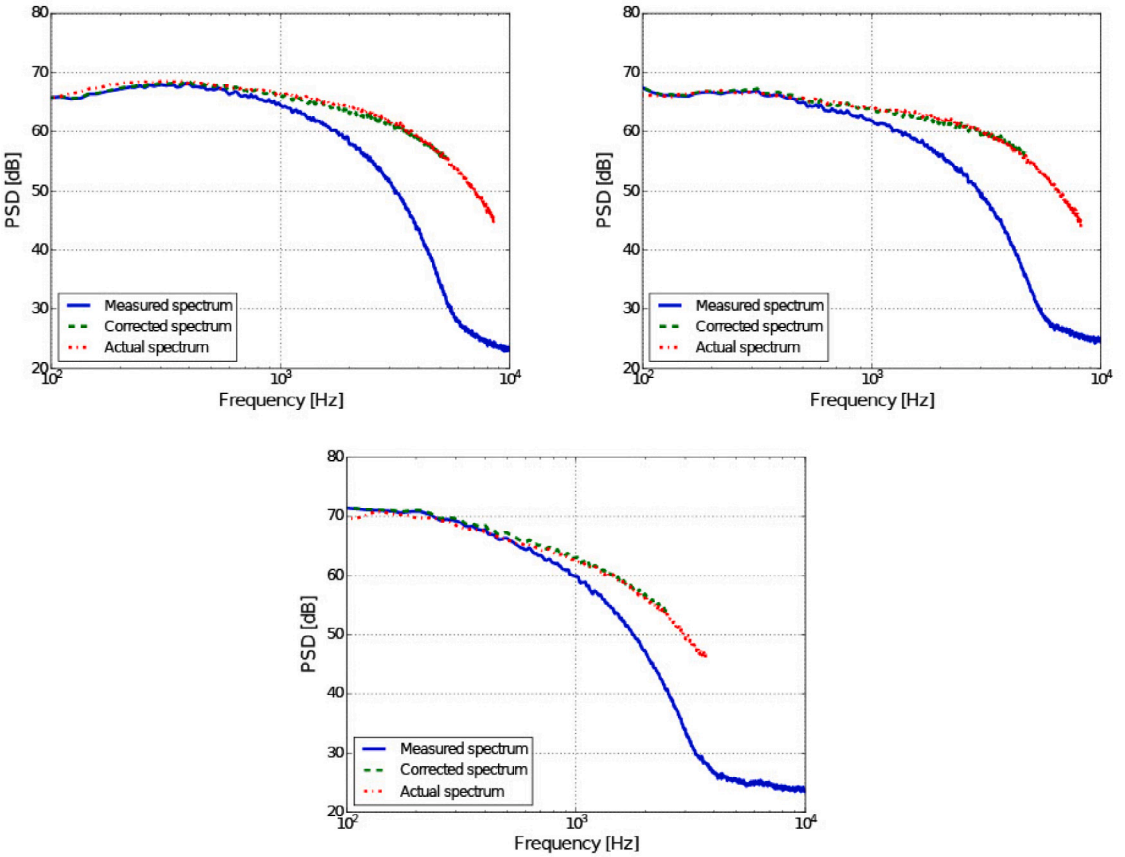

Fig. 24. Measured and corrected wall pressure spectra for a surface sensor at $U_0 = 20$ m/s. (top left) zero pressure gradient (top right) favourable pressure gradient (bottom) adverse pressure gradient.

FISTA solves the inverse problem of source power reconstruction. Hence, the representing neural network gets the measured data as input and outputs the (approximate) solution of the inverse problem. The proposed method modifies the initial sound propagation model, encoded as trainable parameters of the neural network, to correct for the modelling error. This approach is directly applicable to a single measurement i.e. a prior training phase on previously generated data is not required.

The numerical examples show that source power reconstruction results, that are subject to random phase perturbations as modelling error, can be improved. Even though this is still a rather simple synthetic example, the robustness and accuracy of the results with respect to the reconstruction of the source powers $\mathbf{q}$ are remarkable (see Fig. 25). The setup considers $M = 64$ microphones, i.e. $\frac{M(M+1)}{2} = 2080$ correlation data points and $N = 441$ focus points. This leads to $M \cdot N = 28224$ degrees of freedom (DOFs) for the phase perturbation within the residual minimization. Hence, the problem is heavily underdetermined but the correction of the modelling error effects, introduced by random phase perturbations, are possible anyway.

Written by H. Raumer, D. Ernst: daniel.ernst@dlr.de, C. Spehr, DLR, Germany.

5.4. Adaptive RBF with hyperparameter optimization for aeroacoustic applications

In [62], an adaptive metamodelling technique based on the *Radial-Basis-Function* (RBF) is proposed for aeroacoustic applications of highly innovative aircraft layouts. For this class of applications, the designer cannot successfully rely on historical data or low-fidelity models, and the expensive direct simulations remain the only valuable design strategy. The method exploits the stochastic RBF formulation introduced in [63] to evaluate the local metamodel uncertainty, which is used to drive the improvement of the training set with new samples in the more uncertain regions. A procedure to identify the optimal kernel hyperparameters is included in the adaptive scheme, as shown in Fig. 26, to enhance the algorithm's performance and allow to compare kernel functions for which optimal hyperparameter values are difficult to be identified *a priori* as the training set varies at each iteration.

The hyperparameters tuning technique is based on the *Leave-One-Out Cross-Validation* method through Rippa's algorithm [64]. The proposed technique is applied to the case of a simple airfoil in a uniform flow impinged by a point monopole source. The function to be reproduced is the Insertion Loss due to the airfoil shadowing, obtained by solving the convective Helmholtz equation

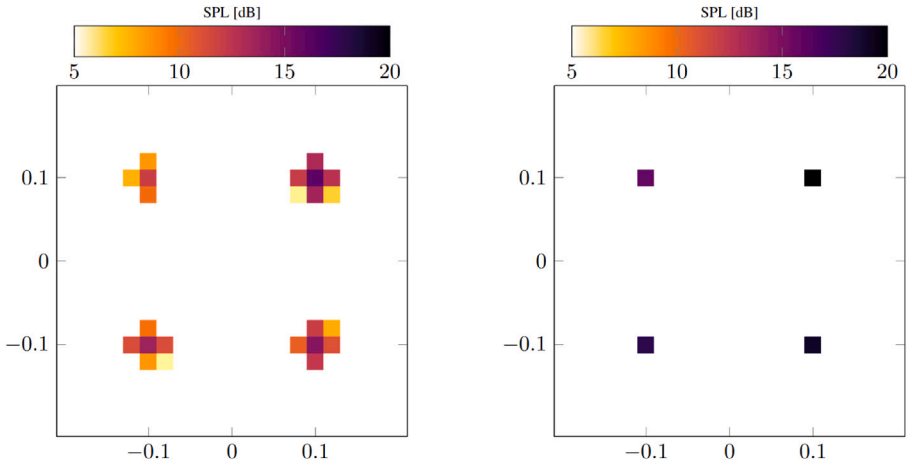

Fig. 25. Solutions for numerical example with random phase perturbation. Left: FISTA solution with perturbed phase ($\|\mathbf{q} - \mathbf{q}^{\dagger}\|_2 = 106.31$). Right: FISTA solution after phase error compensation ($\|\mathbf{q} - \mathbf{q}^{\dagger}\|_2 = 6.56$).

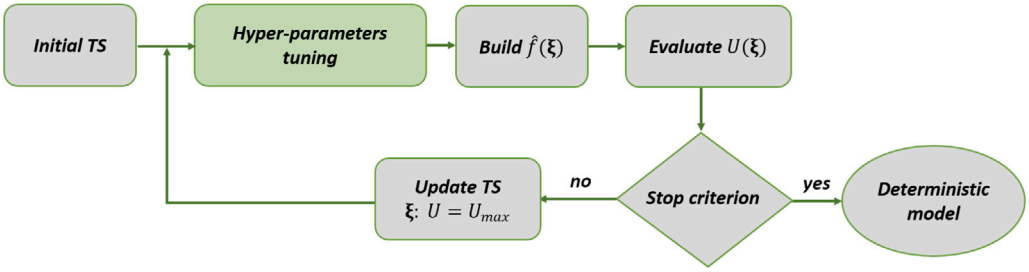

Fig. 26. Flowchart of the dynamic adaptive metamodel update with kernel hyperparameters tuning.

through a BEM solver. The Mach number and the source position are considered design variables. It is proved that using stochastic RBF, a reliable and accurate model of noise shielding can be built using a limited number of simulations. The comparison between metamodels with and without hyperparameter optimization in Fig. 27 for the case of a polynomial spline kernel shows how the presented algorithm greatly helps in reducing the number of points needed to converge, which is an essential feature in the context of Simulation-Based Design.

Written by L. Burghignoli: lorenzo.burghignoli@uniroma3.it, G.Palma, Department of Civil, Computer Science and Aeronautical Technologies Engineering, Roma Tre University, Italy.

5.5. Expert decision support system for aeroacoustic source type identification using clustering

We propose an Expert Decision Support System (EDSS) [65] for the identification of time-invariant, aeroacoustic source types. The system comprises two steps: first, acoustic properties are calculated based on spectral and spatial information. Second, clustering is performed based on these properties. The clustering aims at helping and guiding an expert for quick identification of different source types, providing an understanding of how sources differ. A comparison of the EDSS supported process and the manual analysis process is depicted in Fig. 28.

A variety of features are proposed for capturing the characteristics of the sources. These features represent aeroacoustic properties that can be interpreted by both the machine and by experts. The features are independent of the absolute Mach number which enables the proposed method to cluster data measured at different flow configurations. Fig. 29 shows a projection of the resulting feature space of deconvolved beamforming data of a Do728 [66], and confirms that the proposed features are able to capture enough statistical variance to separate the manually identified source types.

Fig. 30 shows that clustering the sources in the proposed feature space results in groups that mostly correspond to the manually identified source types. The clustering also provides the cluster-averaged feature values, the cluster hierarchy and the clustering confidence. This additional information makes the results transparent, and allows the expert to understand the clustering choices.

Written by Armin Goudarzi: armin.goudarzi@dlr.de, C. Spehr, DLR, and S. Herbold, University of Passau, Germany.

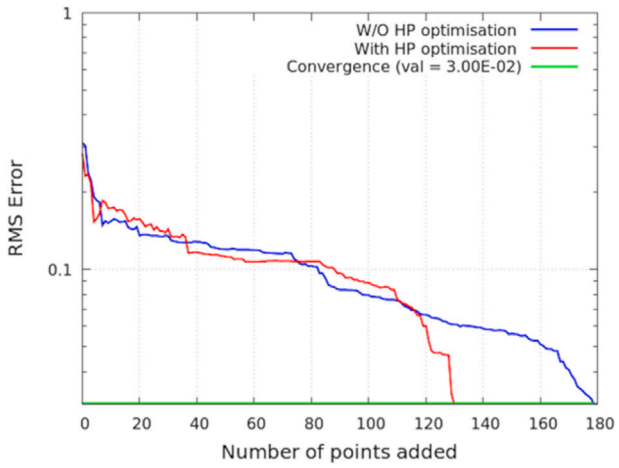

Fig. 27. Comparison between metamodels with and without hyperparameter optimization kernel: polynomial spline frequency band: 630 Hz.

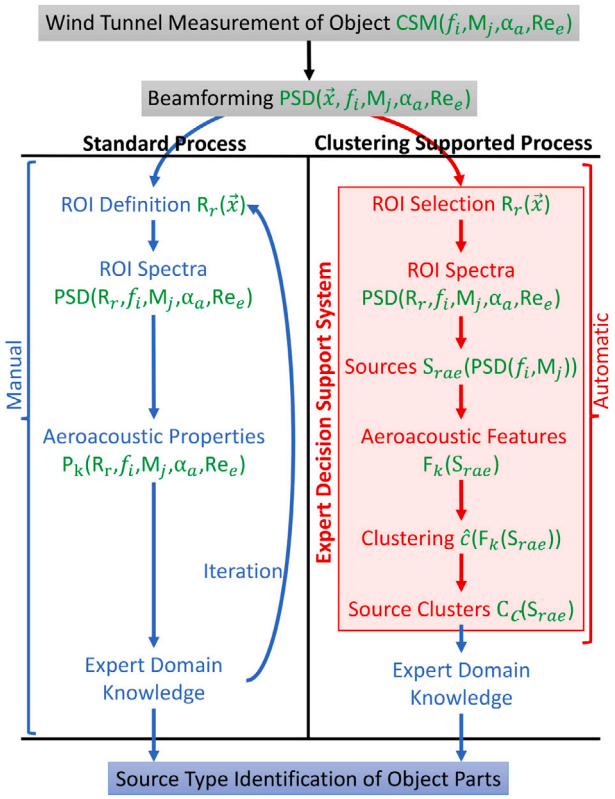

Fig. 28. Comparison of the evaluation process of wind tunnel beamforming measurements. Left: a standard process using manual analysis. Right: the proposed Expert Decision Support System. Manual processing steps are displayed in blue while automatic steps are displayed in red. The resulting variables of each step are displayed in green. The indices indicate the dimensionality of these variables. (For interpretation of the references to colour in this figure legend, the reader is referred to the web version of this article.)

5.6. Extension of the high-resolution CABARET method for computational aeroacoustics problems on rotating grids

For simulations of noise generated by aerodynamic flows, high-resolution numerical methods with small numerical dissipation and dispersion error are required. One example of such methods is CABARET (Compact Accurately Boundary-Adjusting high-REsolution Technique) [67] which was previously accelerated on GPU (Graphics Processing Units) cards and applied for noise calculation of complex high-speed jets [68,69] and airfoil flows Abid et al. [70] on fixed meshes.

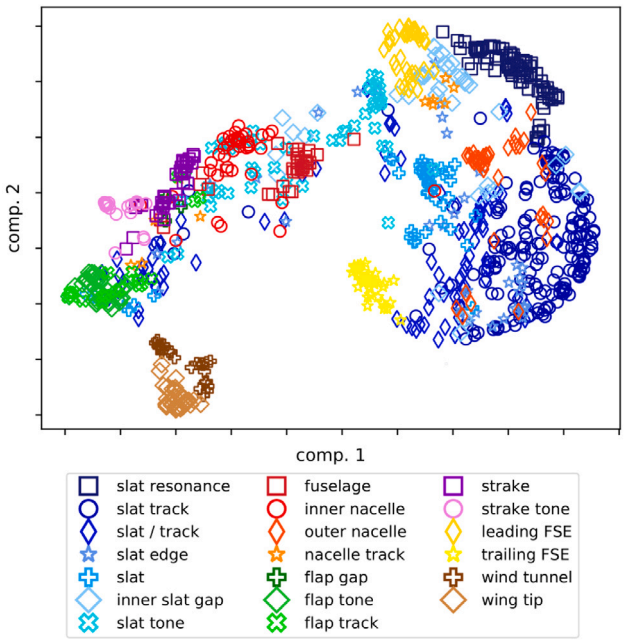

Fig. 29. UMAP feature projection of the Do728 sources with manually identified labels (e.g., slat track). The source distances indicate how similar the features and thus, aeroacoustic properties are.

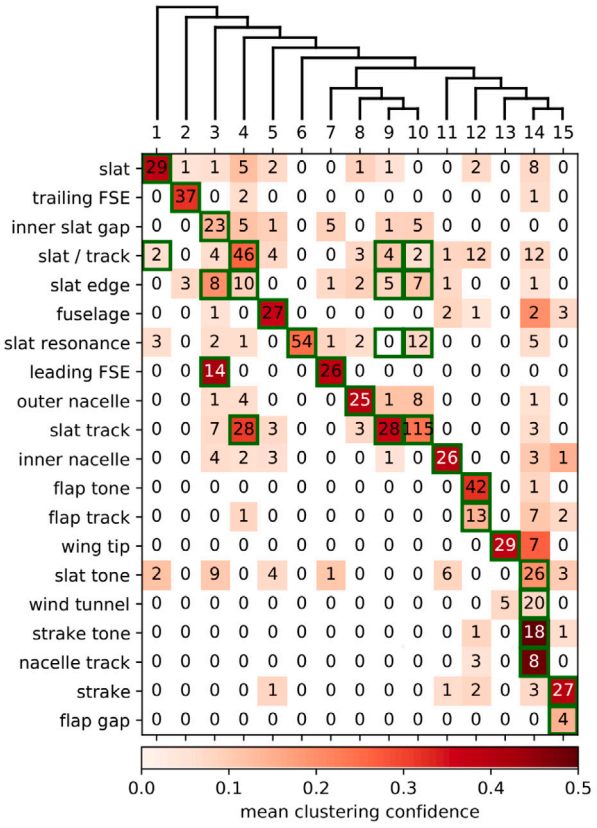

Fig. 30. Confusion matrix of the occurrences of our manually identified source types in the clusters. The colour intensity displays the mean clustering confidence. Cluster choices we consider correct are marked with a green box. The tree above the clusters displays their hierarchy.

In the framework of ENODISE project, CABARET has been extended to rotating grid problems using the sliding interface approach [71]. The developed algorithm ensures a strict preservation of the conservation flux vector through planar and cylindrical sliding interfaces, which is based on the local sub-cell reconstruction of the solution.

Numerical examples are provided for the analytical problem of normal acoustic wave propagation through a rotating cylindrical grid zone embedded in an outer stationary grid. The error decay rates are shown to be consistent with the theoretical order of CABARET convergence. In addition, the same algorithm accelerated on GPUs is applied to simulate the flow around a generic two-bladed rotor corresponding to one of the geometries considered in ENODISE. For two locally refined unstructured meshes considered, 3 and 17 million cells, the time-averaged pressure and velocity solutions are shown to be more-or-less insensitive to the mesh.

The rotor calculations on a single GPU card showed a good computational speed-up: over 24 h 8 rotor revolutions were simulated on the fine grid and 53 rotor revolutions were simulated on the coarse grid. The rapid turn-around time of the developed CABARET method on rotating meshes will allow using it for aeroacoustic rotor optimization studies within a multi-fidelity (coarse grid–fine grid) approach.

Written by I.A. Solntsev, A. Chintagunta, A.P. Markesteijn, S.A. Karabasov: s.karabasov@qmul.ac.uk, Queen Mary University of London, UK.

6. Miscellaneous

6.1. Low-noise design of medium-range aircraft for energy efficient aviation

Domogalla et al. [72] proposed a promising approach for the assessment of a mid-range aircraft design, aiming to reduce atmospheric emissions while simultaneously reducing the noise impact on the ground. The design is based on previous DLR low-noise vehicles [73] and uses a geared turbofan (GTF), combined with a forward-swept wing (FSW) with natural laminar flow (NLF) for low drag, and over the wing-mounted engines for noise shielding [74,75]. The design requirements are based on the top-level aircraft requirements of the cluster of excellence SE^2A [76], aiming to fulfil the EU Flight Path 2050 requirements.

For evaluation, Sound Exposure Level (SEL) noise contours and LA_{max} sideline levels for take-off and approach, as well as CO_2, H_2O, NO_x, and non-volatile Particulate Matter (nvPM) emissions for a 4500 km design mission are assessed. They are compared for a conventional reference design (V-R), a dedicated low-noise design (V-2) and an improved low-noise design using an FSW (V-3). Each of these designs is equipped with a modern GTF engine and a conventional turbofan engine with a bypass ratio of 12 and 6, respectively.

Results show, that the shielding concept using over the wing-mounted engines significantly benefits the noise impact during departure. Especially in combination with a high-bypass ratio GTF noise contours can be reduced by more than 80%, compared to the conventional reference design with BPR-6 engines. The FSW, on the other hand, contributes mostly to the overall fuel consumption, directly effecting the gaseous emissions. While the V-2 design achieves its noise advantage only at the cost of an increased fuel burn, the V-3 design can reduce fuel consumption simultaneously by more than 6% compared to the reference for both engine designs.

Written by Vincent Domogalla: vincent.domogalla@dlr.de, Lothar Bertsch, Martin Plohr, DLR, Germany, Eike Stumpf, RWTH, Aachen, Zoltán S. Spakovszky, MIT, Cambridge.

6.2. Uncertainty quantification for aircraft noise emission simulation: methods and limitations

Aircraft system noise simulation is inherently and inevitably associated with uncertainty. This uncertainty can directly be attributed to (1) the uncertainty of the input data, (2) the uncertainty of the selected emission noise source models, and (3) the uncertainty attributed to sound propagation. Combination of these major effects determines the total uncertainty of the predicted noise levels for the overall aircraft [77]. We have developed several methods for uncertainty assessment in Refs. [77,78], in particular an efficient first-order-second-moment method (FOSM), which has been directly implemented into DLR's PANAM tool [79]. Moreover, we have realized higher order polynomial chaos (PC) surrogates [78], where an existing noise assessment tool can be reused almost in a black box way. The study in [78] provides a direct comparison of the different UQ methods, for the case of the aircraft emission. The approach behind the study is visualized in Fig. 31.

As an example, the predicted standard deviations for an approach situation are depicted in Fig. 32 for a typical case ($s = 1$), with twice ($s = 2$) and three times ($s = 3$) increased input and modelling uncertainties. FOSM results start deviating for large input and modelling uncertainties. Obviously, such large values ($s = 2,3$ ...), while usually not expected in realistic cases, should be avoided by acquiring additional data for instance, as they strongly increase modelling uncertainty.

Finally, a modern fan design (5 dB noise reduction) with twice the input and modelling uncertainty is simulated ("reduced", $s = 2$) and compared with a current design ("original", $s = 1$). This case shows how future technology assessment is affected by uncertainties, see Fig. 33, where the results have been obtained with the PC method.

Written by Ulrich Römer: u.roemer@tu-braunschweig.de, TU Braunschweig, Germany, Lothar Bertsch, DLR, Germany, Sameer B. Mulani, University of Alabama, USA, Beat Schäffer, EMPA, Switzerland.

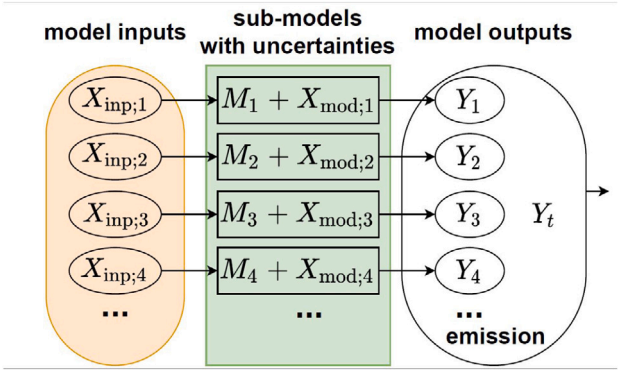

Fig. 31. Schematic of the uncertainty propagation workflow, depicting inputs, outputs, models and their uncertainties.

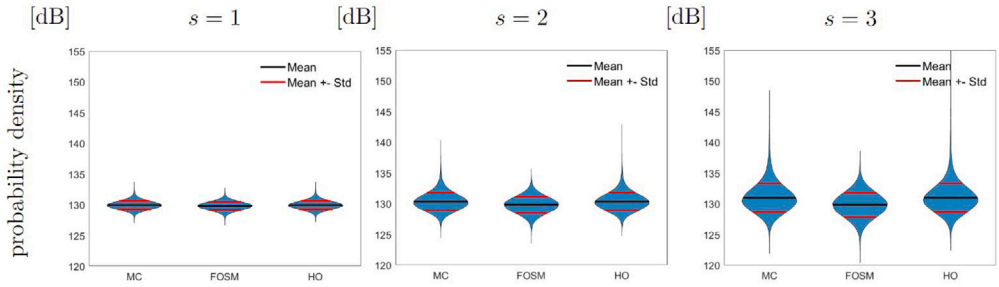

Fig. 32. Comparison of emission probability density functions computed with different methods. Monte Carlo (MC) vs first order second moment (FOSM) vs higher order Polynomial Chaos (HO). Three cases with different sizes of input uncertainty have been considered.

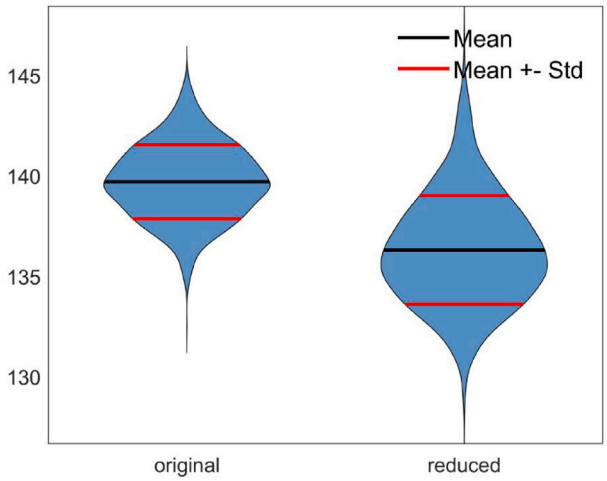

Fig. 33. Future technology assessment under uncertainty. Probability density for a current and future fan technology, where the latter has a reduced emission but a larger modelling uncertainty.

6.3. *Horizon2020 project ARTEM successfully finished*

ARTEM (Aircraft noise Reduction Technologies and related Environmental iMpact) – a 4.5-year European research project funded by the European commission (Horizon2020, Grant 769350) devoted to the development and assessment of novel noise reduction technologies for aircrafts expected to enter service between 2035 and 2050 – ended successfully in May 2022.

ARTEM has successfully explored a large variety of concepts for passive and active noise reduction and associated tools for design, prediction, and evaluation. Two liner concepts, namely the multi-focal and the slanted septum liner concept proved exceptionally good progress. An expected benefit of 0.7–0.9 EPNdB on aircraft level was estimated for a 2025 large long-range aircraft during

the industrial assessment. All other concepts have also made significant progress in maturation reaching the expected TRLs of 3–4 depending on starting point. Shielding modelling has been improved and finally successfully applied – demonstrating the tremendous benefit with respect to noise reductions for ground observers if propulsion systems are placed on top of an aircraft structure – in particular here for blended wing body aircraft.

The complex flow and noise generation phenomena associated with conventional high-lift systems have been successfully modelled and noise reduction by design variations – like the very long chord slat (VLCS) – been demonstrated. The variety of modelling and prediction approaches from quick 2-D tools capable to handle many design variations during an optimization process and high-fidelity simulations including (Overset-)LES for in-depth analysis of noise generation mechanism have been applied and further matured. Other means for noise reductions (serrations, finlets, porous inserts, etc.) have been investigated numerically or experimentally and proved good results on component level, but lower impact during assessment on full aircraft scale.

The boundary layer ingestion concept (BLI), which is anticipated to reduce fuel consumption for "tube&wing" aircraft significantly, has been addressed in a comprehensive study receiving great attention in the community. Tools ranging from low-fidelity modelling to extensive numerical simulations on full aircraft scale using ONERA NOVA and NAUTILIUS platforms have been applied.

It was coherently demonstrated, that the inflow distortions associated with this concept are prone to increase the radiated propulsion noise – mainly fan noise – significantly. Great care is needed in the design of the BLI inlet duct system to reduce inflow distortion as much as possible with extensive application of liners having the capability to further reduce or avoid any noise penalties.

For aircraft landing systems, a large campaign involved experimental and numerical work on detailed source analysis and promising reduction means as meshes, screens, fairing design, and porous inserts. While already demonstrating some potential noise reduction on model scale and during full aircraft assessment, the work performed in ARTEM constitutes a profound basis for on-going H2020 project INVENTOR work.

As a basis for distributed electric propulsion systems, a detailed study of mutual interaction effects of closely spaced rotors, and between rotor and wing structure has been performed. A purpose-build highly modular wind tunnel test setup consisting of a wing section and 3 propellers mountable in pusher and puller configuration was used to build-up a huge experimental data base and subsequent data processing and prediction tool development.

For the early design phase of novel aircraft configurations, a robust multi-dimensional design optimization tool was improved and subsequently applied to design two blended-wing body (BWB) aircraft configurations: BOLT: a long-range BWB, REBEL: a short-range BWB aircraft with either classical UHBR engines (REBEL-C) or a distributed hybrid electrical propulsion system (REBEL-HEP).

The assessment for promising technologies on CleanSky2-derived platforms for short-/medium range (SMR) and long-range (LR) aircraft has been performed by Airbus while a specific business jet platform was used by Dassault Aviation for the same task.

Based on noise predictions of the novel aircraft configurations, auralizations have been generated and used for comparative listening test including also psycho-acoustic aspects of annoyance of future aircraft noise.

A comprehensive overview with references to major scientific publications for each topic is available at the ARTEM website (www.dlr.de/ARTEM) and at the EC website (Publishable summary M48: https://cordis.europa.eu/project/id/769350/results).

Written by Karsten Knobloch, karsten.knobloch@dlr.de, Ralf Burgmayer, DLR, Germany, Eric Manoha, ONERA, France, Francesco Adamo, CIRA, Italy, and Guillaume Bodard, Safran Aircraft Engines, France.

6.4. Horizon2020 project UPWARDS successfully finished

The UPWARDS project (Horizon2020, Grant 763990) has been recently concluded, with the successful implementation of an ambitious research program aimed at enabling the development of bigger and better designed wind turbines, thus increasing the capacity of societies to harness wind-energy. The project has addressed key aspects driving the performance, durability and societal acceptance of large wind turbines. The multi-physic simulation platform developed by the project partners includes the prediction of realistic atmospheric flows via Weather Research Forecast (WRF) simulations and the interactions between the wind turbines via a Park model relying on an Actuator Line Model. The resulting data has served as input to various multi-physics solvers, e.g. for the simulation and optimization of the structural dynamics behaviour of the wind turbine, or for pitch/yaw control and the alleviation of adverse wake interactions between wind turbines in a wind park.

On the aeroacoustics side, Siemens Industry Software (SISW) and the von Karman Institute for Fluid Dynamics (VKI) developed a methodology in order to predict the noise footprint and annoyance levels of wind farms accounting for realistic atmospheric flow conditions.

The simulation flowchart is illustrated in Fig. 34. It starts from high-resolution, unsteady atmospheric flow data, obtained from WRF-LES or Park. The database is then correlated with wind turbine state variables (pitch angle and RPM) which, combined with the wind turbine CAD, permits calculating the detailed flow around the blades. This is performed following a spanwise strip approach, where the motion of each blade segment is approximated by a local rectilinear motion. Two-dimensional RANS simulations provide the necessary input data for the prediction of the blade trailing edge noise emitted by each strip using statistical models (here following Amiet's framework, based on tuned wall pressure semi-empirical models [80]) and stochastic approaches (here the Random Particle Mesh method, [81]). The results are finally recombined for all trips and projected on a near-field control surface from which long-distance acoustic propagation is obtained using a ray-tracing tool, enabling an assessment of the level of annoyance caused by the wind turbine or wind farm [82]. The noise prediction methodology has been validated on the benchmark of a SWT2.3MW-93 wind turbine located on the Høvsøre test centre and that contains meteorological mast data, wind turbine state and noise measurements [83].

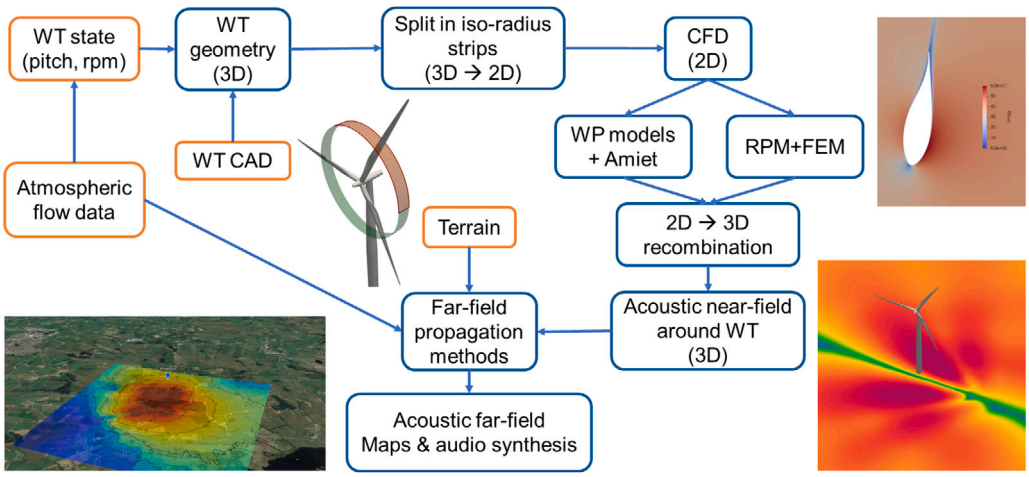

Fig. 34. Wind turbine noise simulation flowchart.

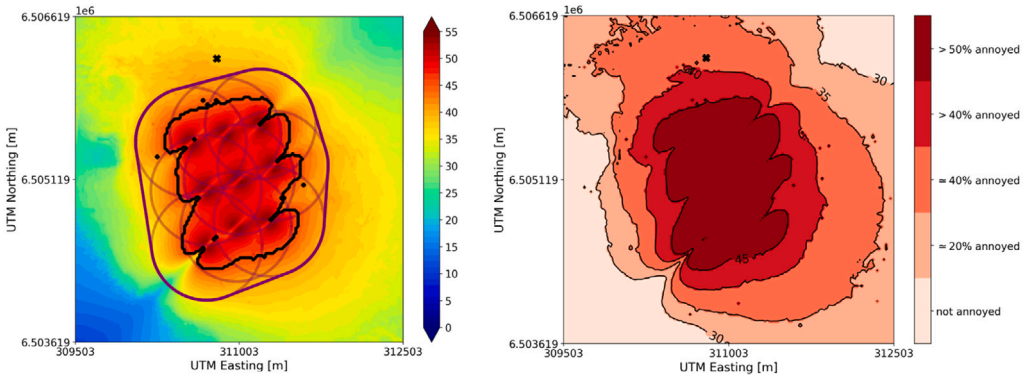

Fig. 35. Noise footprint and annoyance map calculated for the Høgjaeren wind park in Norway.

This methodology has been also demonstrated for a subset of 9 wind turbines of the Høgjaeren wind park in Norway. The noise computation takes as input the weather reforecast simulation of the 30th Dec., 2017 and the park simulation accounting for the wind turbines interactions. As an output (Fig. 35), the overall sound pressure level map is provided on a listener grid around the wind farm overlayed with the set-back distance (circles around wind turbines) and noise threshold (black iso-contour) defining the noise regulations in Norway. Working together with Wageningen University, corresponding annoyance maps are computed showing the percentage of people likely to be annoyed by the wind turbine noise. The available noise methodology can be used to optimize the wind turbine layout and individual wind turbine operational parameters in order to minimize the noise footprint. [82].

Written by Christophe Schram, christophe.schram@vki.ac.be, Julien Christophe, VKI, Belgium, Sophie Le Bras, Hadrien Bériot, SISW, Belgium.

6.5. Advancements on wind turbine aeroacoustics research

Wind turbine noise is still an open area of research. For on-shore applications, research on improving the design of conventional or novel noise reduction technologies, such as trailing edge serrations, and the execution of benchmarks to improve both high and low-fidelity models [84] is still active. For example, Lima Pereira et al. [85,86], by performing surface pressure measurements on an airfoil equipped with trailing-edge serrations, have suggested a physics-based description of how the flow alter the surface pressure fluctuation intensity over a serration and has provided semi-empirical methods to account for that.

In alternative to large-scale wind turbines, small scale ones, such as vertical axis wind turbines (VAWT) can be used in urban environments. Brandetti et al. [87] have performed LBM-VLES simulations of a realistic VAWT, also tested experimentally, to assess the predictive capability of a low-fidelity method based on coupling the actuator cylinder model with semi-empirical noise prediction tools. Results have shown that the low-fidelity method can be consider accurate for the preliminary design phase, but three dimensionality effects must be accounted for in the final design phase, for both acoustics and aerodynamics.

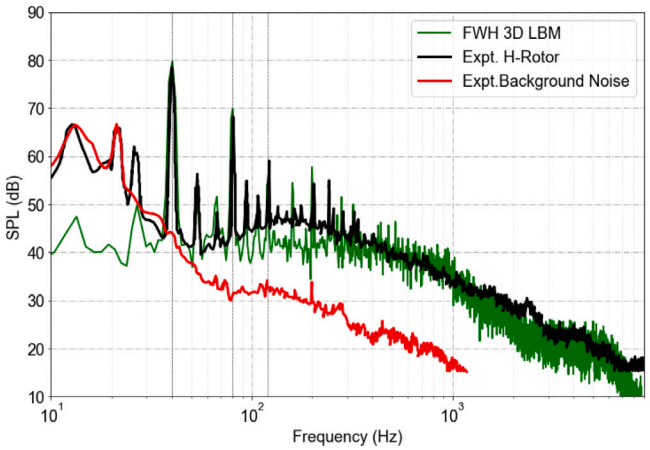

Fig. 36. Noise spectra for a observer position located 1 m away for the Deep stall regime.

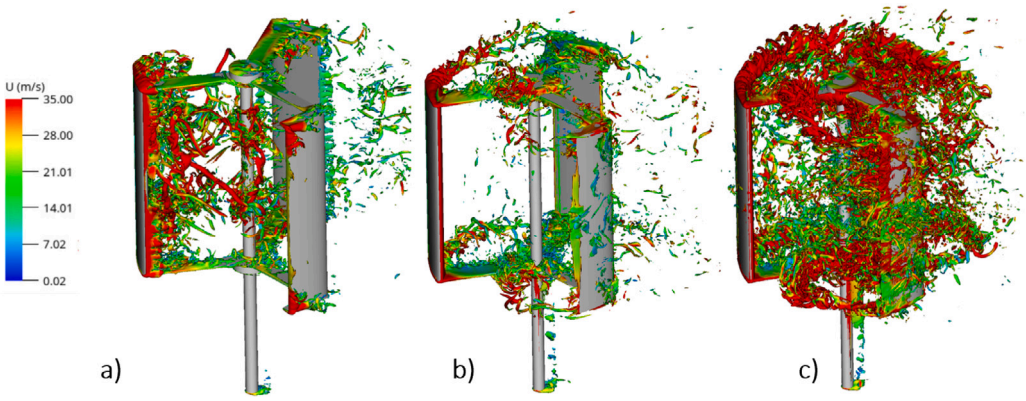

Fig. 37. Iso-surfaces of Q-criterion for different flow regimes (a) Deep stall regime (800 rpm) (b) Operational regime (3500 rpm) (c) Parasitic drag regime (6000 rpm).

Wind energy is developing strongly offshore. Here, aerodynamic generated noise can be used as a maintenance tool to minimize the inspection time and maximize energy production. Zhang et al. [88] have shown that relevant aeroacoustics features can be detected but, when incoming turbulence with large amplitude is present, aeroacoustics measurements must be coupled with other techniques, such as IR thermography.

Written by Francesco Avallone, francesco.avallone@polito.it, Politecnico di Torino, Italy, and Daniele Ragni, Delft University of Technology, Netherlands.

6.6. Numerical investigation of noise radiated by vertical axis wind turbines using LBM approach

The aerodynamics and aeroacoustics of a scale model H-Darrieus VAWT with end plates and support structures were studied for various flow conditions (TSR). A 3D Lattice Boltzmann simulation was performed to predict the sound pressure levels at the observer position, and these were compared to available experimental data. The results showed good agreement with both the tonal peaks and broadband levels in both the dynamic stall (as seen in Fig. 36) and operational regimes.

Complex noise generation mechanisms are seen due to dynamic stall and blade wake interactions over the azimuthal revolution. As TSR increases, the OASPL and noise directivity also increase. In the operational regime, key flow structures are near the blade tips and interact with end plates as shown in Fig. 37. As TSR continues to increase, corresponding to the parasitic drag regime, blade wake interactions and flow mixing increase, resulting in increased broadband noise levels.

Further details on the aerodynamic and aeroacoustics characters in each flow regime of the turbine are discussed in Refs. [89–92].

Written by Kartik Venkatraman, kartik.venkatraman@vki.ac.be, VKI, Belgium, Christophe Schram, VKI, Belgium, and Stéphane Moreau, Université de Sherbrooke, Canada. *The financial support of the European Commission, provided in the framework of the H2020 zEPHYR project (Marie Skłodowska-Curie grant agreement No 860101), is gratefully acknowledged.*

6.7. On the Rossiter–Heller frequency of resonant cavities

Following a validation effort of the transonic Lattice Boltzmann Method (LBM) flow solver SIMULIA PowerFLOW Mancini et al. [93], the aeroacoustic properties of rectangular cavities were investigated with the intent of improving the Rossiter–Heller resonance frequency formula Casalino et al. [94]. A database of LBM results covering different Mach numbers and cavity aspect ratios was used to define a fitting formula for the backward flow velocity inside the cavity used to correct the travel time of the backward propagating wave. Inclusion of this corrective term in the formula led to a significant improvement of the resonance frequency prediction. Furthermore, the nature of additional tones occurring in a deep cavity with aspect ratio of 5 in supersonic regime was deeply scrutinized through non-linear spectral analysis, wavelet/frequency filtering and spectral POD. All the results confirmed the hypothesis of non-linear mode coupling leading to an amplitude modulation.

Written by Damiano Casalino, damanio.casalino@3ds.com, Dassault Systemes Deutschland GmbH, Germany.

Declaration of competing interest

The authors declare that they have no known competing financial interests or personal relationships that could have appeared to influence the work reported in this paper.

Data availability

Data will be made available on request.

References

[1] M. van Nesselrooij, L. Veldhuis, B. van Oudheusden, F. Schrijer, Drag reduction by means of dimpled surfaces in turbulent boundary layers, Exp. Fluids 57 (2016) 1–14, http://dx.doi.org/10.1007/s00348-016-2230-9, URL: https://link.springer.com/article/10.1007/s00348-016-2230-9.

[2] P. Spalart, M. Shur, M. Strelets, A. Travin, K. Paschal, S. Wilkinson, Experimental and numerical study of the turbulent boundary layer over shallow dimples, Int. J. Heat Fluid Flow 78 (2019) 108438, http://dx.doi.org/10.1016/j.ijheatfluidflow.2019.108438, URL: https://www.sciencedirect.com/science/article/abs/pii/S0142727X19302176.

[3] V. Ananthan, R. Akkermans, T. Hu, P. Liu, N. Ratje, Trailing-edge noise reduction potential of a locally applied shallow dimpled surface, J. Sound Vib. 525 (2022) 116745, http://dx.doi.org/10.1016/j.jsv.2022.116745, URL: https://www.sciencedirect.com/science/article/abs/pii/S0022460X22000025.

[4] R. Akkermans, P. Bernicke, R. Ewert, J. Dierke, Zonal overset-LES with stochastic volume forcing, Int. J. Heat Fluid Flow 70 (2018) 336–347, http://dx.doi.org/10.1016/j.ijheatfluidflow.2017.11.005, URL: https://www.sciencedirect.com/science/article/abs/pii/S0142727X1730379X.

[5] S. Oerlemans, P. Sijtsma, B. Méndez López, Location and quantification of noise sources on a wind turbine, J. Sound Vib. (2007) 15, http://dx.doi.org/10.1016/j.jsv.2006.07.032.

[6] A. Manso Jaume, J. Wild, Aerodynamic design and optimization of a high-lift device for a wind turbine airfoil, in: A. Dillmann, G. Heller, E. Krämer, C. Wagner, C. Breitsamter (Eds.), New Results in Numerical and Experimental Fluid Mechanics X, Vol. 132, Springer International Publishing, Cham, 2016, pp. 859–869, http://dx.doi.org/10.1007/978-3-319-27279-5_75.

[7] A. Suryadi, C. Jätz, J. Seume, M. Herr, Identifying the flap side-edge noise contribution of a wind turbine blade section with an adaptive trailing edge, Wind Energy 26 (1) (2023) 64–75, http://dx.doi.org/10.1002/we.2786, URL: https://onlinelibrary.wiley.com/doi/abs/10.1002/we.2786.

[8] A. Suryadi, F. Schmidt, C. Appel, N. Reiche, R. Ewert, M. Herr, J. Wild, Noise simulations of flap devices for wind turbine rotors, Wind Energy 26 (1) (2023) 23–43, http://dx.doi.org/10.1002/we.2784, URL: https://onlinelibrary.wiley.com/doi/abs/10.1002/we.2784.

[9] N. Reiche, R. Ewert, M. Lummer, J. Delfs, Fast multipole boundary element method with stochastic sources for broadband noise simulation, in: 23rd AIAA/CEAS Aeroacoustics Conference, American Institute of Aeronautics and Astronautics, Denver, Colorado, 2017, http://dx.doi.org/10.2514/6.2017-3515.

[10] C. Appel, B. Fassmann, S.Y. Lin, M. Herr, CAA-basierte Schallvorhersage für Windkraftanlagen, in: Fortschritte der Akustik - DAGA 2020, in: Tagungsband DAGA, Deutsche Gesellschaft für Akustik e.V., Hannover, 2020, p. 4.

[11] T.F. Geyer, E. Sarradj, Circular cylinders with soft porous cover for flow noise reduction, Exp. Fluids 57 (2016) 1–16.

[12] T.F. Geyer, Experimental evaluation of cylinder vortex shedding noise reduction using porous material, Exp. Fluids 61 (2020) 1–21.

[13] T.F. Geyer, Effect of a porous coating on the vortex shedding noise of a cylinder in turbulent flow, Appl. Acoust. 195 (2022) 108834.

[14] S. Sharma, T.F. Geyer, E.J. Arcondoulis, On the influence of porous coating thickness and permeability on passive flow and noise control of cylinders, J. Sound Vib. (2023) 117563.

[15] E.J. Arcondoulis, T.F. Geyer, Y. Liu, An investigation of wake flows produced by asymmetrically structured porous coated cylinders, Phys. Fluids 33 (3) (2021) 037124.

[16] E.J. Arcondoulis, T.F. Geyer, Y. Liu, An acoustic investigation of non-uniformly structured porous coated cylinders in uniform flow, J. Acoust. Soc. Am. 150 (2) (2021) 1231–1242.

[17] R. Zamponi, S. Satcunanathan, S. Moreau, D. Ragni, M. Meinke, W. Schröder, C. Schram, On the role of turbulence distortion on leading-edge noise reduction by means of porosity, J. Sound Vib. (2020-07) 115561, http://dx.doi.org/10.1016/j.jsv.2020.115561.

[18] S. Tamaro, R. Zamponi, D. Ragni, C. Teruna, C. Schram, Experimental investigation of turbulent coherent structures interacting with a porous airfoil, Exp. Fluids 62 (2021) 94, http://dx.doi.org/10.1007/s00348-021-03170-2.

[19] R. Zamponi, Investigation of Turbulence-Surface Interaction Noise Mechanisms and Their Reduction Using Porous Materials (Ph.D. thesis), Delft University of Technology, 2021, http://dx.doi.org/10.4233/uuid:d332c7e3-87be-4ed6-aa71-e629ef77e07a.

[20] R. Zamponi, S. Satcunanathan, S. Moreau, M. Meinke, W. Schroeder, C. Schram, Investigation of curle's dipolar sources on a porous airfoil interacting with incoming turbulence, in: 28th AIAA/CEAS Aeroacoustics 2022 Conference, American Institute of Aeronautics and Astronautics, 2022-06-14, http://dx.doi.org/10.2514/6.2022-2985.

[21] R. Zamponi, S. Satcunanathan, S. Moreau, M. Meinke, W. Schröder, C. Schram, Effect of porosity on Curle's dipolar sources on an aerofoil in turbulent flow, J. Sound Vib. 542 (2023-01) 117353, http://dx.doi.org/10.1016/j.jsv.2022.117353.

[22] R. Zamponi, S. Moreau, C. Schram, Rapid distortion theory of turbulent flow around a porous cylinder, J. Fluid Mech. 915 (2021-05-25) A27, http://dx.doi.org/10.1017/jfm.2021.8.

[23] T. Zhang, D. Moreau, T. Geyer, J. Fischer, C. Doolan, Dataset on tip vortex formation noise produced by wall-mounted finite airfoils with flat and rounded tip geometries, Data Brief 28 (2020) 105058.

[24] E. Schneehagen, T.F. Geyer, E. Sarradj, D.J. Moreau, Aeroacoustic noise reduction by application of end plates on wall-mounted finite airfoils, Exp. Fluids 62 (5) (2021) 106.
[25] E.W. Schneehagen, T.F. Geyer, E. Sarradj, Influence of end plate placement on the reduction of airfoil tip vortex formation noise, Acta Acust. 6 (2022) 59.
[26] D. Casalino, E. Grande, G. Romani, D. Ragni, F. Avallone, Definition of a benchmark for low Reynolds number propeller aeroacoustics, Aerosp. Sci. Technol. 113 (2021).
[27] E. Grande, G. Romani, D. Ragni, F. Avallone, D. Casalino, Aeroacoustic investigation of a propeller operating at low-Reynolds number, AIAA J. 60 (2) (2022) 860–871.
[28] E. Grande, D. Ragni, F. Avallone, D. Casalino, Laminar separation bubble noise on a propeller operating at low Reynolds numbers, AIAA J. 60 (9) (2022).
[29] G. Romani, E. Grande, F. Avallone, D. Ragni, D. Casalino, Performance and noise prediction of low-Reynolds number propellers using the lattice-Boltzmann method, Aerosp. Sci. Technol. 125 (2021) 107086.
[30] G. Romani, E. Grande, F. Avallone, D. Ragni, D. Casalino, Computational study of flow incidence effects on the aeroacoustics of low blade-tip mach number propellers, Aerosp. Sci. Technol. 120 (2022) 107275.
[31] D. Casalino, G. Romani, R. Zhang, H. Chen, Lattice-Boltzmann calculations of rotor aeroacoustics in transitional boundary layer regime, Aerosp. Sci. Technol. 130 (2022) 107953.
[32] Y. Fuerkaiti, E. Grande, D. Casalino, F. Avallone, D. Ragni, Efficient low-fidelity aeroacoustic permanence calculation of propellers, Aerosp. Sci. Technol. 123 (2022) 107438.
[33] C. Poggi, G. Bernardini, M. Gennaretti, R. Camussi, Scalability of mach number effects on noise emitted by side-by-side propellers, Appl. Sci. 12 (2022) 9507, http://dx.doi.org/10.3390/app12199507.
[34] M. Gennaretti, G. Bernardini, Novel boundary integral formulation for blade-vortex interaction aerodynamics of helicopter rotors, AIAA J. 45 (2007) 1169–1176, http://dx.doi.org/10.2514/1.18383.
[35] M. Gennaretti, G. Bernardini, J. Serafini, G. Romani, Rotorcraft comprehensive code assessment for blade–vortex interaction conditions, Aerosp. Sci. Technol. 80 (2018) 232–246, http://dx.doi.org/10.1016/j.ast.2018.07.013.
[36] C. Poggi, G. Bernardini, M. Gennaretti, Aeroacoustic analysis of wing-mounted propeller arrays, in: AIAA AVIATION 2021 Forum, in: AIAA 2021-2236, AIAA, 2021, http://dx.doi.org/10.2514/6.2021-2236, Virtual Event.
[37] C. Poggi, M. Rossetti, J. Serafini, G. Bernardini, M. Gennaretti, U. Iemma, Neural network meta–modelling for an efficient prediction of propeller array acoustic signature, Aerosp. Sci. Technol. 130 (2022) 107910, http://dx.doi.org/10.1016/j.ast.2022.107910.
[38] C. Poggi, M. Rossetti, G. Bernardini, U. Iemma, C. Andolfi, C. Milano, M. Gennaretti, Surrogate models for predicting noise emission and aerodynamic performance of propellers, Aerosp. Sci. Technol. 125 (2022) 107016, http://dx.doi.org/10.1016/j.ast.2021.107016.
[39] G. Bernardini, F. Centracchio, M. Gennaretti, U. Iemma, C. Pasquali, C. Poggi, M. Rossetti, J. Serafini, Numerical characterisation of the aeroacoustic signature of propeller arrays for distributed electric propulsion, Appl. Sci. 10 (2020) 2643, http://dx.doi.org/10.3390/app10082643.
[40] P. Chaitanya, P. Joseph, D. Akiwate, A. Parry, S. Prior, On the noise generation mechanisms of overlapping propellers, in: AIAA AVIATION 2021 Forum, in: AIAA 2021-2281, AIAA, 2021, http://dx.doi.org/10.2514/6.2021-2281, Virtual Event.
[41] P. Chaitanya, P. Joseph, S. Prior, A. Parry, On the optimum separation distance for minimum noise of contra-rotating rotors, J. Sound Vib. 535 (117032) (2022) http://dx.doi.org/10.1016/j.jsv.2022.117032, URL: https://www.sciencedirect.com/science/article/pii/S0022460X22002504?via%3Dihub.
[42] P. Chaitanya, P. Joseph, T.P. Chong, M. Priddin, L. Ayton, On the noise reduction mechanisms of porous aerofoil leading edges, J. Sound Vib. 485 (115574) (2020) http://dx.doi.org/10.1016/j.jsv.2020.115574, URL: https://www.sciencedirect.com/science/article/pii/S0022460X20304065.
[43] S. Palleja-Cabre, C.C. Paruchuri, P. Joseph, M.J. Priddin, L.J. Ayton, Downstream perforations for the reduction of turbulence-aerofoil interaction noise: Part I - Experimental investigation, in: AIAA AVIATION 2021 Forum, in: AIAA 2021-2149, AIAA, 2021, http://dx.doi.org/10.2514/6.2021-2149, Virtual Event.
[44] M.J. Priddin, L.J. Ayton, S. Palleja-Cabre, P. Chaitanya, P. Joseph, Downstream perforations for the reduction of turbulence-aerofoil interaction noise: Part II - Theoretical investigation, in: AIAA AVIATION 2021 Forum, in: AIAA 2021-2147, AIAA, 2021, http://dx.doi.org/10.2514/6.2021-2147, Virtual Event.
[45] S. Palleja-Cabre, P. Chaitanya, P. Joseph, J.W. Kim, M.J. Priddin, L.J. Ayton, T.F. Geyer, T.P. Chong, Downstream porosity for the reduction of turbulence-aerofoil interaction noise, J. Sound Vib. 541 (117324) (2022) http://dx.doi.org/10.1016/j.jsv.2022.117324, URL: https://www.sciencedirect.com/science/article/pii/S0022460X22005077.
[46] R. Roncen, F. Méry, E. Piot, P. Klotz, Spatially-varying impedance model for locally reacting acoustic liners at a high sound intensity, J. Sound Vib. (2022) 116741, http://dx.doi.org/10.1016/j.jsv.2021.116741.
[47] W. Eversman, Effect of local impedance variation and non-linearity on multiple tone attenuation, Int. J. Aeroacoustics 14 (1–2) (2015) 281–303, http://dx.doi.org/10.1260/1475-472X.14.1-2.281.
[48] R. Billard, G. Gabard, M. Versaevel, G. Tissot, A non-linear impedance model for micro-perforated liners, in: e-Forum Acusticum 2020, 2020, URL: https://hal.inria.fr/hal-03143278/document.
[49] Y. Renou, Y. Aurégan, Failure of the Ingard–Myers boundary condition for a lined duct: An experimental investigation, J. Acoust. Soc. Am. 130 (1) (2011) 52–60, http://dx.doi.org/10.1121/1.3586789.
[50] M. Shur, M. Strelets, A. Travin, T. Suzuki, P. Spalart, Unsteady simulations of sound propagation in turbulent flow inside a lined duct, AIAA J. 59 (8) (2021) http://dx.doi.org/10.2514/1.J060181.
[51] L. Casadei, T. Node-Langlois, H. Deniau, E. Piot, C. Polacsek, Acoustic mode attenuation in ducts using CFD with time-domain impedance boundary condition, AIAA J. 60 (12) (2022) http://dx.doi.org/10.2514/1.J061879.
[52] F. Monteghetti, D. Matignon, E. Piot, L. Pascal, Design of broadband time-domaine impedance boundary conditions using the oscillatory-diffusive representation of acoustical models, J. Acoust. Soc. Am. 140 (3) (2016) 1663–1674, http://dx.doi.org/10.1121/1.4962277.
[53] M. Yang, P. Sheng, Sound absorption structures: From porous media to acoustic metamaterials, Annu. Rev. Mater. Res. 47 (2017) 83–114, http://dx.doi.org/10.1146/annurev-matsci-070616-124032, URL: https://www.annualreviews.org/doi/10.1146/annurev-matsci-070616-124032.
[54] M.J. Bianco, P. Gerstoft, J. Traer, E. Ozanich, M.A. Roch, S. Gannot, C.A. Deledalle, Machine learning in acoustics: Theory and applications, J. Acoust. Soc. Am. 146 (5) (2019) 3590–3628, http://dx.doi.org/10.1121/1.5133944.
[55] A. Casaburo, D. Magliacano, G. Petrone, F. Franco, S. De Rosa, Gaussian-based machine learning algorithm for the design and characterization of a porous meta-material for acoustic applications, Appl. Sci. 12 (1) (2022) http://dx.doi.org/10.3390/app12010333, URL: https://www.mdpi.com/2076-3417/12/1/333.
[56] N. Hu, Sensor-size-related attenuation correction of wall pressure spectra measurements, Phys. Fluids 34 (2022) 1–21, http://dx.doi.org/10.1063/5.0094847.
[57] G.M. Corcos, Resolution of pressure in turbulence, J. Acoust. Soc. Am. 35 (2) (1963) 192–199, http://dx.doi.org/10.1121/1.1918431.
[58] H.-G. Raumer, D. Ernst, C. Spehr, Compensation of modeling errors for the aeroacoustic inverse problem with tools from deep learning, Acoustics 4 (4) (2022) 834–848, http://dx.doi.org/10.3390/acoustics4040050, URL: https://www.mdpi.com/2624-599X/4/4/50.
[59] G.H. Golub, P.C. Hansen, D.P. O'Leary, Tikhonov regularization and total least squares, SIAM J. Matrix Anal. Appl. 21 (1) (1999) 185–194, http://dx.doi.org/10.1137/s0895479897326432.
[60] A. Beck, M. Teboulle, A fast iterative shrinkage-thresholding algorithm for linear inverse problems, SIAM J. Imaging Sci. 2 (1) (2009) 183–202, http://dx.doi.org/10.1137/080716542.

[61] S. Dittmer, T. Kluth, P. Maass, D.O. Baguer, Regularization by architecture: A deep prior approach for inverse problems, J. Math. Imaging Vision 62 (3) (2019) 456–470, http://dx.doi.org/10.1007/s10851-019-00923-x.
[62] L. Burghignoli, M. Rossetti, F. Centracchio, G. Palma, U. Iemma, Adaptive RBF with hyperparameter optimisation for aeroacoustic applications, Int. J. Aeroacoustics 21 (1–2) (2022) 22–42, http://dx.doi.org/10.1177/1475472X221079545.
[63] S. Volpi, M. Diez, N. Gaul, H. Song, U. Iemma, K. Choi, E. Campana, F. Stern, Development and validation of a dynamic metamodel based on stochastic radial basis functions and uncertainty quantification, Struct. Multidiscip. Optim. 51 (2) (2015) 347, 368, http://dx.doi.org/10.2514/3.13046.
[64] S. Rippa, An algorithm for selecting a good value for the parameter c in radial basis function interpolation, Adv. Comput. Math. 11 (1999) 193–210, http://dx.doi.org/10.1023/A:1018975909870.
[65] A. Goudarzi, C. Spehr, S. Herbold, Expert decision support system for aeroacoustic source type identification using clustering, J. Acoust. Soc. Am. 151 (2) (2022) 1259–1276, http://dx.doi.org/10.1121/10.0009322.
[66] A. Goudarzi, C. Spehr, S. Herbold, Automatic source localization and spectra generation from sparse beamforming maps, J. Acoust. Soc. Am. 150 (3) (2021) 1866–1882, http://dx.doi.org/10.1121/10.0005885.
[67] S. Karabasov, V. Goloviznin, Compact accurately boundary-adjusting high-resolution technique for fluid dynamics, J. Comput. Phys. 228 (2009) 7426–7451, http://dx.doi.org/10.1016/j.jcp.2009.06.037, URL: https://www.sciencedirect.com/science/article/pii/S0021999109003684.
[68] A. Markesteijn, S. Karabasov, Simulations of co-Axial jet flows on graphics processing units: the flow and noise analysis, Philos. Trans. R. Soc. A Math. Phys. Eng. Sci. 377 (2019) 2159, http://dx.doi.org/10.1098/rsta.2019.0083, URL: https://royalsocietypublishing.org/doi/10.1098/rsta.2019.0083.
[69] A. Markesteijn, V. Gryazev, S. Karabasov, R. Ayupov, L. Benderskiy, D. Lyubimov, Flow and noise predictions of coaxial jets, Am. Inst. Aeronaut. Astronaut. AIAA J. 58 (2020) 5280–5293, http://dx.doi.org/10.2514/1.J058881, URL: https://arc.aiaa.org/doi/10.2514/1.J058881.
[70] H. Abid, A. Markesteijn, S. Karabasov, Trailing edge noise modelling of flow over NACA airfoils informed by LES, in: AIAA AVIATION 2021 Forum, in: AIAA 2021-2233, AIAA, 2021, http://dx.doi.org/10.2514/6.2021-2233, Virtual Event.
[71] I. Solntsev, A. Chintagunta, A. Markesteijn, S. Karabasov, CABARET on rotating meshes, Appl. Math. Comput. 446 (2023) 127871, http://dx.doi.org/10.1016/j.amc.2023.127871, URL: https://www.sciencedirect.com/science/article/pii/S0096300323000401?dgcid=coauthor.
[72] V. Domogalla, L. Bertsch, M. Plohr, E. Stumpf, Z.S. Spakovszky, Low-noise design of medium-range aircraft for energy efficient aviation, Aerospace 9 (1) (2022) http://dx.doi.org/10.3390/aerospace9010003, URL: https://www.mdpi.com/2226-4310/9/1/3.
[73] L. Bertsch, F. Wolters, W. Heinze, M. Pott-Pollenske, J. Blinstrub, System Noise Assessment of a Tube-and-Wing Aircraft with Geared Turbofan Engines, AIAA J. Aircr. 56 (4) (2019) 1577–1596, http://dx.doi.org/10.2514/1.C034935.
[74] M. Hepperle, Environmental friendly transport aircraft, in: C. Breitsamter, B. Laschka, H.J. Heinemann, R. Hilbig (Eds.), New Results in Numerical and Experimental Fluid Mechanics IV, Vol. 4, No. 1, Springer Berlin Heidelberg, Berlin, Heidelberg, 2004, pp. 26–33.
[75] G. Redeker, G. Wichmann, Forward sweep-A favorable concept for a laminar flow wing, J. Aircr. 28 (2) (1991) 97–103.
[76] J. Friedrichs, SE2A - Sustainable and Energy-Efficient Aviation, Cluster of Excellence, Full Proposal, TU Braunschweig, Braunschweig, Germany, 2018.
[77] L. Bertsch, B. Schäfer, S. Guerin, Uncertainty analysis for parametric aircraft system noise prediction, in: Aerospace Research Central (Ed.), J. Aircr. 56 (2) (2019) 529–544, http://dx.doi.org/10.2514/1.C034809, ISSN 0021-8669 (print) or 1533-3868 (online).
[78] U. Römer, L. Bertsch, S.B. Mulani, B. Schäffer, Uncertainty quantification for aircraft noise emission simulation: Methods and limitations, in: AIAA (Ed.), AIAA J. 60 (5) (2022) 3020–3034, http://dx.doi.org/10.2514/1.J061143.
[79] L. Bertsch, L. Sanders, R.H. Thomas, I. LeGriffon, J.C. June, I.A. Clark, M. Lorteau, Comparative assessment of aircraft system noise simulation, in: AIAA (Ed.), J. Aircr. 58 (4) (2021) 867–884, http://dx.doi.org/10.2514/1.C036124, eISSN 1533-3868.
[80] Y.C. Küçükosman, J. Christophe, C. Schram, Trailing edge noise prediction based on wall pressure spectrum models for NACA0012 airfoil, J. Wind Eng. Ind. Aerodyn. 175 (2018) 305–316.
[81] A. Kadar, S. Le Bras, H. Bériot, C.F. Schram, V. Korchagin, W. De Roeck, W. Desmet, Airfoil trailing-edge noise prediction combining a random particle-mesh method with a Helmholtz solver, in: 2018 AIAA/CEAS Aeroacoustics Conference, 2018, p. 3596.
[82] A. Bresciani, J. Maillard, L. de Santana, Perceptual evaluation of wind turbine noise, in: 16ème Congrès Français d'Acoustique, CFA2022, 2022.
[83] J. Christophe, S. Buckingham, C. Schram, S. Oerlemans, zEPHYR - Large On Shore Wind Turbine Benchmark, Zenodo, 2022, http://dx.doi.org/10.5281/zenodo.6380879.
[84] S. Luesutthiviboon, L.T. Lima Pereira, D. Ragni, F. Avallone, M. Snellen, Aeroacoustic benchmarking of trailing-edge noise from NACA 633–018 airfoil with trailing-edge serrations, AIAA J. 61 (2022) 329–354, http://dx.doi.org/10.2514/1.J061630.
[85] L.T. Lima Pereira, D. Ragni, F. Avallone, F. Scarano, Aeroacoustics of sawtooth trailing-edge serrations under aerodynamic loading, J. Sound Vib. 537 (2022) 117202, http://dx.doi.org/10.1016/j.jsv.2022.117202.
[86] L.T. Lima Pereira, F. Avallone, D. Ragni, F. Scarano, A physics-based description and modelling of the wall-pressure fluctuations on a serrated trailing edge, J. Fluid Mech. 938 (2022) A28, http://dx.doi.org/10.1017/jfm.2022.173.
[87] L. Brandetti, F. Avallone, D. De Tavernier, B. LeBlanc, C. Simao Ferreira, D. Casalino, Assessment through high-fidelity simulations of a low-fidelity noise prediction tool for a vertical-axis wind turbine, J. Sound Vib. 547 (2023) 117486, http://dx.doi.org/10.1016/j.jsv.2022.117486.
[88] Y. Zhang, F. Avallone, S. Watson, Wind turbine blade trailing edge crack detection based on airfoil aerodynamic noise: An experimental study, Appl. Acoust. 191 (2022) 108668, http://dx.doi.org/10.1016/j.apacoust.2022.108668.
[89] K. Venkatraman, S. Moreau, J. Christophe, C. Schram, Numerical investigation of the effect of inflow non-uniformity on the noise radiated by a vertical axis wind turbine, in: AIAA AVIATION Forum, in: AIAA 6.2021-2216, 2021, http://dx.doi.org/10.2514/6.2021-2216, Online.
[90] K. Venkatraman, S. Moreau, J. Christophe, C. Schram, H-darrieus vertical axis wind turbine power prediction using the lattice Boltzmann approach, in: 56th 3AF International Conference on Applied Aerodynamics, Toulouse, France, 2022.
[91] K. Venkatraman, S. Moreau, J. Christophe, C. Schram, Numerical investigation of the noise radiated by an H-darrieus vertical axis wind turbine at different tip speed ratios, in: 28th AIAA/CEAS Aeroacoustics Conference, Southampton, in: AIAA 2022-3058 paper, 2022.
[92] K. Venkatraman, S. Moreau, J. Christophe, C. Schram, Numerical Investigation of H Darrieus wind turbine aerodynamics at different tip speed ratios, Internat. J. Numer. Methods Heat Fluid Flow (2023) http://dx.doi.org/10.1108/HFF-09-2022-0562.
[93] S. Mancini, A. Kolb, I. Gonzalez-Martino, D. Casalino, Predicting high-speed feedback mechanisms in rectangular cavities using lattice-Boltzmann very-large eddy simulations, Aerosp. Sci. Technol. 117 (2) (2021).
[94] D. Casalino, I. Gonzalez-Martino, S. Mancini, A. Kolb, On the rossiter-heller frequency of resonant cavities, Aerosp. Sci. Technol. 131 (2022) 108013.